An Analysis of the Riemann Problem for a 2×2 System of Keyfitz-Kranzer Type Conservation Laws Using Shadow Waves and Dafermos Regularization

Josh Culver *[1], Aubrey Ayres †[2], Evan Halloran‡[3], Ryan Lin §[4], Emily Peng ¶[5], and Charis Tsikkou ‖[4]

[1]Department of Mathematics, Purdue University, West Lafayette, IN 47907, USA
[2]Department of Mathematics, University of South Carolina, Columbia, SC 29208, USA
[3]Department of Mathematics, Indiana University, Bloomington, IN 47405, USA
[4]School of Mathematical and Data Sciences, West Virginia University, Morgantown, WV 26506, USA
[5]Department of Physics, Yale University, New Haven, CT 06511, USA

February 16, 2026

Abstract

We investigate a system of two conservation laws and analyze the self-similar Riemann solutions, encompassing both classical and non-classical wave patterns. A key outcome is the existence of overcompressive delta-shocks, which arise as singular limits through Dafermos regularization of the system. Although structurally simple, the model encapsulates the essential mechanisms of transport under density constraints, making it a flexible prototype for crowd-limited dynamics observed in settings such as traffic flow, granular media, ecological dispersal, and biological aggregation. To capture the internal shock structure, we employ blow-up methods within the framework of Geometric Singular Perturbation Theory (GSPT). Theoretical predictions are further validated by numerical simulations based on the local Lax-Friedrichs scheme.

Key Words. Conservation Laws; Self-Similar Solutions; Unbounded Solutions; Delta-Shocks; Dafermos Regularization; Geometric Singular Perturbation Theory; Asymptotic Analysis; Riemann Problems; Dynamical Systems; Blow-up; Degenerate Hyperbolicity; Nonconvex Flux; Granular Compaction; Crowd Dynamics; Nonlinear Population Dynamics

AMS Subject Classifications. 34A05, 34C37, 34C45, 34E15, 35L45, 35L65, 35L67, 35L80, 35Q92, 65M06, 74L10, 76A30

1 Introduction

This work focuses on a nonlinear system of two conservation laws modeling transport under density dependence in the absence of external forcing (for the case where a time-dependent external force is incorporated,

*culver23@purdue.edu †aayres@email.sc.edu ‡ehallor@iu.edu §rl00023@mix.wvu.edu ¶emily.peng@yale.edu ‖tsikkou@math.wvu.edu

see Culver et al. [5]). The system takes the form:

$$\rho_t + \left(\rho u \left(1 - \left(\frac{\rho}{\bar{\rho}}\right)^a\right)\right)_x = \rho_t + \big(f_1(\rho, u)\big)_x = 0, \tag{1.1}$$

$$(\rho u)_t + \left(\rho u^2 \left(1 - \left(\frac{\rho}{\bar{\rho}}\right)^a\right)\right)_x = (\rho u)_t + \big(f_2(\rho, u)\big)_x = 0, \tag{1.2}$$

where the dependent variables are density ρ and velocity u. The constant $\bar{\rho} > 0$ is a critical density (for example, a jamming or saturation threshold) and $a \in \mathbb{R}\setminus\{0\}$ governs the nonlinear degeneracy of the mobility term. The sign of a has significant modeling and analytical consequences: For $a > 0$, mobility vanishes as $\rho \to \bar{\rho}$, modeling crowding or jamming effects due to high density; for $a < 0$, degeneracy occurs as $\rho \to 0$, modeling low-density inhibition such as clustering or dispersal suppression. Throughout the paper ρ is interpreted as a density variable. Although the equations are mathematically meaningful for arbitrary real values of ρ, we focus on Riemann data with $\rho > 0$. All analytical constructions and numerical experiments presented here seem to preserve nonnegative density; a general invariant-region analysis is beyond the scope of this work.

Although this system has a simple structure and does not include complex effects, it serves as a versatile prototype for transport processes affected by crowding or depletion effects, with applications in biological aggregation, ecological dispersal, traffic flow, and granular compaction. A key analytical feature of the model is the loss of strict hyperbolicity. The characteristic speeds of the system are

$$\lambda_a = u\left(1 - (a+1)\left(\frac{\rho}{\bar{\rho}}\right)^a\right), \quad \lambda_0 = u\left(1 - \left(\frac{\rho}{\bar{\rho}}\right)^a\right),$$

and, depending on the state, can coincide or vanish. In particular, degeneracy occurs along the critical density surface $\rho = \bar{\rho}$, where $\lambda_0 = 0$, along $\rho = \bar{\rho} \cdot (\frac{1}{a+1})^{1/a}$ when $a > -1$, where $\lambda_a = 0$, partially degeneracy occurs at $\rho = 0$ when $a > 0$, where the system loses strict hyperbolicity and the two eigenvalues are equal, and full degeneracy occurs at $u = 0$, where both eigenvalues vanish. This breakdown of strict hyperbolicity gives rise to novel behaviors. One characteristic field of the system is linearly degenerate, while the other is genuinely nonlinear (see Section 2.1), which shapes the geometry of wave interactions, leading to contact discontinuities and, in combination with the degenerate flux structure, allowing the formation of overcompressive δ-shock solutions.

We construct and classify self-similar Riemann solutions, capturing both classical wave patterns (contact discontinuities, rarefactions, and shocks) and non-classical ones, such as overcompressive delta-shocks that arise as bona fide limits of smooth solutions to the Dafermos regularization and possess internal structure that can be resolved using blow-up techniques from Geometric Singular Perturbation Theory. In addition to the singular solutions mentioned above, which are the main focus of this work, the Riemann problem also admits solutions that pass through vacuum states ($\rho = 0$) and across the critical density threshold $\rho = \bar{\rho}$, where mobility vanishes and one characteristic speed degenerates. A comprehensive treatment of all wave patterns is presented in Culver et al. [5]. Our analytical results are validated through numerical simulations using the local Lax–Friedrichs scheme, which confirms the emergence of singular profiles, vacuum layers, and degenerate wave transitions predicted by the theory.

In one space dimension, the Riemann problem is fundamental in understanding solutions to a Cauchy problem in systems of conservation laws. For this reason, explicit constructions of Riemann solutions are of both theoretical and computational importance. From a modeling perspective, a δ-shock represents the concentration of mass along a moving interface. The singular measure describes the limiting behavior of increasingly localized high-density regions rather than a breakdown of the conservation structure.

A rigorous justification of these singular structures was later supplied by Schecter [28], who constructed viscous self-similar profiles, using geometric singular perturbation theory and a blow-up method to resolve the loss of normal hyperbolicity. This framework is based on the geometric methods of Fenichel [7] and Jones [10]. For further developments and related approaches to singular solutions, see also [9, 11, 12, 14, 15, 16, 19, 20] and the references therein.

Previous investigations of singular solutions have primarily focused on cases where only a single state variable concentrates into a Dirac delta distribution. However, physically relevant systems exist in which both state variables simultaneously develop singularities. For example, in two-component chromatography,

studied numerically by Mazzotti et al. [21, 22, 23], both components of the conserved variables concentrate and neither component satisfies the classical Rankine–Hugoniot condition. Tsikkou [31] further analyzed this system by applying linear transformations to conserved quantities, derived a simplified system that was subsequently studied, and provided a coherent explanation for the observed unbounded solutions.

Other extensions include balance law models with external forcing. Frew et al. [8], for example, studied a Keyfitz–Kranzer-type system involving a generalized Chaplygin gas with a time-dependent source term. Their analysis revealed a family of classical and non-classical singular solutions whose admissibility changes in time as a result of the forcing. More broadly, recent investigations (see Culver et al. [5]) demonstrate that singular phenomena are not confined to autonomous systems; time-dependent and non-conservative effects can also generate rich behavior with applications in gas dynamics, cosmology, and reactive flows.

These results highlight a set of open questions. Under what structural conditions do singularities arise, and what principles govern their admissibility? In what sense do such solutions satisfy the conservation law, and how can generalized frameworks extend the notion of weak solutions? Finally, how are these effects tied to degeneracy, non-hyperbolicity, or the breakdown of genuine nonlinearity?

The system considered in this paper addresses these issues. It is physically motivated while also serving as a mathematically tractable example where non-classical and singular wave patterns appear in degenerate regimes. From a mathematical point of view, this work seeks to expand the understanding of how singular solutions can serve as essential building blocks in the global resolution of Riemann and Cauchy problems with large initial data, potentially leading to new solution theories and generalized numerical schemes.

The system consisting of equations (1.1) and (1.2) is a special case of

$$\begin{cases} \rho_t + \Big(\rho\Phi\big(\rho,u\big)\Big)_x = F\big(\rho,u\big), \\ \big(\rho u\big)_t + \Big(\rho u\Phi\big(\rho,u\big)\Big)_x = G\big(\rho,u\big), \end{cases} \tag{1.3}$$

and has various applications depending on Φ, F, and G. For example, the pressureless Euler system and a simplified second-order traffic flow model structurally related to simplified versions of the Aw and Rascle [1] and Zhang [33] models correspond to $F = G = 0$, $\Phi(\rho,u) = u$, and $F = G = 0$, $\Phi(\rho,u) = u - p(\rho)$, respectively. The literature, such as in Zhang [34, 35], shows that the Riemann problem with pressure laws depending solely on density and with $F = 0$ has been extensively studied.

Systems of the form (1.3) belong to the broader class of Keyfitz-Kranzer-type conservation laws, introduced in the seminal work of Keyfitz and Kranzer [13] in the context of nonstrictly hyperbolic elasticity models admitting singular shock solutions. Such systems are characterized by fluxes which are colinear with the state vectors, typically written as

$$u_t + \big(\Phi(u)\,u\big)_x = 0, \qquad u \in \mathbb{R}^n,$$

where Φ is a scalar function of the state variables, and provide canonical examples of models exhibiting concentration phenomena and overcompressive waves. Such systems have been studied extensively both in the homogeneous case [2, 4, 26] and in balance-law extensions with source terms [29, 32]. The present model incorporates a power-law dependence through the exponent a, which modifies the nonlinear structure of the flux and leads to new admissibility features in the associated Riemann problem.

In this work, we consider equations (1.1) and (1.2) and describe solutions to the Riemann problem. The initial data are given by

$$(\rho,u)(x,0) = \begin{cases} (\rho_L,u_L) & x < 0, \\ (\rho_R,u_R) & x > 0, \end{cases} \tag{1.4}$$

which represents a jump discontinuity between two constant states in a strictly hyperbolic region. The limiting case $a = 0$ corresponds formally to a degenerate transport regime related to sticky-particle dynamics. Although not pursued here, we mention this case to situate the model within the broader class of degenerate Keyfitz-Kranzer-type systems.

The careful analysis of Riemann problems and the geometry of the Hugoniot locus has become central in recent developments in the theory of conservation laws. Recent multidimensional studies have demonstrated

the possibility of non-uniqueness of admissible weak solutions in models related to compressible flow; see, for example, Březina, Kreml and Mácha [3]. In a different direction, Nedeljkov and Ružiči [25], showed that even classical overcompressibility conditions may fail to ensure uniqueness in generalized Chaplygin-type systems. Investigating whether the present analytical framework can be used to formulate refined uniqueness criteria remains an interesting direction for future research.

The main novelty of the present work is to provide a unified analytical framework for the Riemann problem in a class of systems with power-law nonlinear flux. The dependence on the exponent a plays a crucial role in the structure of admissible solutions, leading to a systematic classification of solution regimes and clarifying the structure of overcompressive waves within the model. In addition, the analysis combines complementary perspectives: two distributional formulations that make precise the sense in which the singular solutions solve the equations, together with a constructive existence mechanism based on the underlying geometric structure of the system, which provides a consistent interpretation of the resulting δ-shock profiles.

The paper is organized as follows: In Section 2, we provide a formal description of the classical Riemann solutions to the system of conservation laws. We derive the shock and contact discontinuity curves through a given left state using the Rankine–Hugoniot conditions, and construct the rarefaction curves based on the system's eigenvalues and eigenvectors. In Section 3, we verify that singular solutions satisfy equations (1.1) and (1.2) in the sense of distributions. There are two standard approaches to this verification. One is to directly postulate a solution involving Dirac delta distributions and substitute it into the weak formulation using test functions. The other, known as the shadow wave method, was introduced by Marko Nedeljkov [6, 24, 25] and involves the construction of a family of smooth approximate solutions with narrow internal layers that concentrate as singular limits. In Section 4, we present state space plots for various values of $a \in \mathbb{R} \setminus \{0\}$, and identify the regions in which the Riemann problem cannot be solved using only shocks, contact discontinuities, and rarefactions. In Section 5, we apply the method of Geometric Singular Perturbation Theory (GSPT) combined with blow-up techniques to resolve the internal structure of the unbounded self-similar profiles that arise from the Dafermos regularization. Finally, in Section 6, we summarize our main findings and outline possible directions for future work.

Notation

We define $[\cdot] := [\cdot]_{\text{jump}} = \cdot_L - \cdot_R$, or $\cdot_- - \cdot_+$.

2 Classical Waves: Contact Discontinuities, Shocks, and Rarefactions

In this section, we start by calculating the eigenvalues of the system and examining how the property of strict hyperbolicity varies with the state. Next, we determine the Hugoniot locus, which is the set of points in state space that can be connected to a fixed left state by either a shock wave that meets the Lax admissibility condition or a contact discontinuity. We also identify the a-rarefaction curve, representing the set of points in the state space that can be connected through an a-rarefaction. In Section 4, we plot the Hugoniot locus and discuss various combinations of classical wave patterns.

2.1 Hyperbolicity, Genuine Nonlinearity, and Linear Degeneracy

We will eventually separate cases based on the value of a, but initial calculations can generally proceed. We start by writing the system of (1.1) and (1.2) in vector form as $\partial_t H + \partial_x G = 0$, where $H(\rho, u, x, t) = (\rho \;\; \rho u)^T$ and

$$G = \begin{pmatrix} \rho u - \rho u \left(\frac{\rho}{\bar{\rho}}\right)^a \\ \rho u^2 - \rho u^2 \left(\frac{\rho}{\bar{\rho}}\right)^a \end{pmatrix}.$$

For a general vector $(B_1 \;\; B_2)^T$ we define

$$D\begin{pmatrix} B_1 \\ B_2 \end{pmatrix} = \begin{pmatrix} \frac{\partial B_1}{\partial \rho} & \frac{\partial B_1}{\partial u} \\ \\ \frac{\partial B_2}{\partial \rho} & \frac{\partial B_2}{\partial u} \end{pmatrix}.$$

To determine whether our system is hyperbolic, we seek eigenvalues and eigenvectors, that is, λ and R such that $(DG - \lambda DH)R = 0$. Note that

$$DG - \lambda DH = \begin{pmatrix} u - (a+1)u\left(\frac{\rho}{\bar{\rho}}\right)^a - \lambda & \rho - \rho\left(\frac{\rho}{\bar{\rho}}\right)^a \\ \\ u^2 - (a+1)u^2\left(\frac{\rho}{\bar{\rho}}\right)^a - \lambda u & 2\rho u - 2\rho u\left(\frac{\rho}{\bar{\rho}}\right)^a - \lambda\rho \end{pmatrix}. \tag{2.1}$$

Solving $\det(DG - \lambda DH) = 0$ yields

$$0 = \left(\lambda + u\left((a+1)\left(\frac{\rho}{\bar{\rho}}\right)^a - 1\right)\right)\left(\lambda + u\left(\left(\frac{\rho}{\bar{\rho}}\right)^a - 1\right)\right).$$

As we will see, the order of these two eigenvalues changes according to the sign of $a \cdot u$ ($\lambda_a < \lambda_0$ if $a \cdot u > 0$; both quantities are defined precisely below), so we label them to denote their form rather than "one" and "two" to denote their order. Thus,

$$\lambda_a = u\left(1 - (a+1)\left(\frac{\rho}{\bar{\rho}}\right)^a\right), \tag{2.2}$$

$$\lambda_0 = u\left(1 - \left(\frac{\rho}{\bar{\rho}}\right)^a\right). \tag{2.3}$$

We note that the eigenvalues are real, $\lambda_a \neq \lambda_0$ for $a \neq 0$ and neither are identically zero when $u \neq 0$, $\rho \neq \bar{\rho}$, $\rho \neq \bar{\rho} \cdot (\frac{1}{a+1})^{1/a}$ (when $a > -1$), and $\rho \neq 0$; thus, our system is strictly hyperbolic. In view of $\nabla\lambda_0 \cdot r_0 = 0$, the quantity λ_0 behaves as a Riemann invariant for the linearly degenerate family, a fact that motivates the alternative characteristic variables discussed in the remark at the end of this subsection. After a short calculation, we obtain the corresponding eigenvectors,

$$R_a = \begin{pmatrix} 1 \\ 0 \end{pmatrix}, \tag{2.4}$$

$$R_0 = \begin{pmatrix} \rho\left(1 - \left(\frac{\rho}{\bar{\rho}}\right)^a\right) \\ \\ au\left(\frac{\rho}{\bar{\rho}}\right)^a \end{pmatrix}. \tag{2.5}$$

Finally, observe that

$$D\lambda_a \cdot R_a = -u\frac{(a+1)a\rho^{a-1}}{\bar{\rho}^a}, \tag{2.6}$$

$$D\lambda_0 \cdot R_0 = -u\frac{a\rho^a}{\bar{\rho}^a}\left(1 - \left(\frac{\rho}{\bar{\rho}}\right)^a\right) + a\left(\frac{\rho}{\bar{\rho}}\right)^a u\left(1 - \left(\frac{\rho}{\bar{\rho}}\right)^a\right) = 0. \tag{2.7}$$

Hence, the a-characteristic family is genuinely nonlinear unless $a = -1$ or $u = 0$, and the 0-characteristic family is linearly degenerate. Consequently, the 0-family generates contact discontinuities, while the a-family produces shocks or rarefactions depending on the ordering of characteristic speeds.

As a quick digression, we note the already common appearance of a and $a+1$. These hint that our cases will separate using the sign of these two values: $a < -1$, $a = -1$, $-1 < a < 0$, and $0 < a$.

Remark 1. *As shown the 0-characteristic family is linearly degenerate, so motivated by this structure, one may introduce the variable $p := \lambda_0(\rho, u)$, (and a complementary variable q) to rewrite the system in a form that emphasizes transport along the 0-family. In particular, for self-similar solutions this change of variables can simplify the description of rarefaction waves (e.g. $p(\xi)$ becomes linear in $\xi = x/t$ in the corresponding rarefaction regime). We note, however, that shock and δ-shock dynamics are most naturally expressed in the original conservative variables $(\rho, \rho u)$, and we therefore retain the (ρ, u) formulation throughout the main analysis.*

2.2 Rankine-Hugoniot Jump Conditions and Related Calculations

We seek conditions on pairs of points in the $(\rho, u)-$plane such that there exists a shock wave propagating at speed s and satisfying the Rankine–Hugoniot jump conditions, which connects the two states. However, because we have a system of two variables, we consider both equations (1.1) and (1.2) and require $s = x'(t), x : \mathbb{R} \to \mathbb{R}$ such that

$$\begin{cases} s[\rho] = \left[\rho u - \rho u \left(\frac{\rho}{\bar{\rho}}\right)^a\right], \\ s[\rho u] = \left[\rho u^2 - \rho u^2 \left(\frac{\rho}{\bar{\rho}}\right)^a\right]. \end{cases} \tag{2.8}$$

Assuming $[\rho] \neq 0$ and $[\rho u] \neq 0$, this means that, given a left state (ρ_L, u_L), we try to find all pairs (ρ_R, u_R) such that

$$\begin{aligned} &\frac{\rho_L u_L - \rho_L u_L \left(\frac{\rho_L}{\bar{\rho}}\right)^a}{\rho_L - \rho_R} - \frac{\rho_R u_R - \rho_R u_R \left(\frac{\rho_R}{\bar{\rho}}\right)^a}{\rho_L - \rho_R} \\ &= \frac{\rho_L u_L^2 - \rho_L u_L^2 \left(\frac{\rho_L}{\bar{\rho}}\right)^a}{\rho_L u_L - \rho_R u_R} - \frac{\rho_R u_R^2 - \rho_R u_R^2 \left(\frac{\rho_R}{\bar{\rho}}\right)^a}{\rho_L u_L - \rho_R u_R}. \end{aligned}$$

Although this is algebraically impossible in general, we show that by considering certain curves of the form $u = f(u_L, \rho_L, \rho)$ one obtains either a shock or a contact discontinuity for each characteristic family. This allows us to identify all shock and contact discontinuity curves in the (ρ, u)-plane.

From this point forward, we denote the right state variables ρ_R and u_R as ρ and u, since we view them as variable points in the state space, with ρ_L and u_L fixed.

2.2.1 Shock and Rarefaction Curves of the a-Family: $a \neq -1$

Consider $u_L = u \neq 0$ and $a \neq -1$. Then (2.8) is satisfied by ρ_L and ρ, and

$$s_a = u_L \left\{1 - \frac{\left(\rho_L \left(\frac{\rho_L}{\bar{\rho}}\right)^a - \rho \left(\frac{\rho}{\bar{\rho}}\right)^a\right)}{\rho_L - \rho}\right\}. \tag{2.9}$$

The a-shock satisfies the Lax shock admissibility criterion if

$$\lambda_a(\rho, u) < s_a < \lambda_a(\rho_L, u_L), \tag{2.10}$$

that is, the shock speed must be between the characteristic speeds on either side of the discontinuity. The condition is equivalent to requiring that characteristics of the a-family enter the shock from both sides, ensuring that the shock is compressive. This is equivalent to

$$\begin{cases} (a+1)\rho^a > \frac{\left(\rho_L^{a+1} - \rho^{a+1}\right)}{\rho_L - \rho} > (a+1)\rho_L^a & \text{if } u_L = u > 0, \\ (a+1)\rho^a < \frac{\left(\rho_L^{a+1} - \rho^{a+1}\right)}{\rho_L - \rho} < (a+1)\rho_L^a & \text{if } u_L = u < 0. \end{cases} \tag{2.11}$$

Further calculations allow us to obtain Table 1.

	$a < -1$	$-1 < a < 0$	$0 < a$
$u_L = u > 0$	S_a to the right	S_a to the left	S_a to the right
$u_L = u < 0$	S_a to the left	S_a to the right	S_a to the left

Table 1: Existence of classical shocks of the a-family when $u = u_L$

where S_a denotes the a-family shock curve. Notice that, in verifying the Lax shock admissibility criterion for $a \neq -1$, the inequalities are exactly reversed on the opposite side of the left state, i.e., $\lambda_a(\rho, u) > s_a > \lambda_a(\rho_L, u_L)$ for some values of (ρ, u). Recalling that the a-family is genuinely nonlinear, we expect a rarefaction curve, a self-similar solution that continuously connects the left and right states when the characteristics fan out. We now proceed to derive its explicit form.

Let $\xi = \frac{x}{t}$ (refer to the beginning of Section 5 for details) so that (1.1) and (1.2) become

$$(DG - \xi DH) \begin{pmatrix} \frac{\mathrm{d}\rho}{\mathrm{d}\xi} \\ \\ \frac{\mathrm{d}u}{\mathrm{d}\xi} \end{pmatrix} = 0. \tag{2.12}$$

Since this rarefaction is to be of the a-family, we set $\xi = \frac{x}{t} = \lambda_a$ and require $\begin{pmatrix} \frac{\mathrm{d}\rho}{\mathrm{d}\xi} \\ \\ \frac{\mathrm{d}u}{\mathrm{d}\xi} \end{pmatrix}$ to equal an eigenvector of the a-family, i.e., any multiple of the eigenvector R_a from (2.4). Let this multiple be a function $f(\rho, u)$. Then

$$\begin{pmatrix} \frac{\mathrm{d}\rho}{\mathrm{d}\xi} \\ \\ \frac{\mathrm{d}u}{\mathrm{d}\xi} \end{pmatrix} = \begin{pmatrix} f(\rho, u) \\ \\ 0 \end{pmatrix} = f(\rho, u) R_a.$$

If $F_R(\rho, D_2) = \int \frac{1}{f(\rho, D_2)}\, d\rho$, we have $F_R\big(\rho(\xi), D_2\big) = \xi + D_1$ and $u(\xi) = D_2$ for some $D_1, D_2 \in \mathbb{R}$. For this to connect the left state to the right state, we require

$$\begin{aligned} F_R(\rho_L, u_L) &= \lambda_a(\rho_L, u_L) + D_1, \\ F_R(\rho, u) &= \lambda_a(\rho, u) + D_1, \\ u_L &= D_2 = u. \end{aligned}$$

This means $F_R(\rho_L, u_L) - F_R(\rho, u) = \lambda_a(\rho_L, u_L) - \lambda_a(\rho, u)$. Thus, we see that $F_R(\rho, u) = \lambda_a(\rho, u)$ and $D_1 = 0$ suffice. Rarefaction curves, when they exist, are defined by

$$(\rho, u)(x, t) = (\rho, u)\left(\frac{x}{t}\right) = \begin{cases} (\rho_L, u_L) & \xi < \lambda_a(\rho_L, u_L), \\ \left(\overline{\rho}\left(\frac{u_L - \xi}{(a+1)u_L}\right)^{\frac{1}{a}}, u_L\right) & \lambda_a(\rho_L, u_L) \leq \xi \leq \lambda_a(\rho, u), \\ (\rho, u_L) & \lambda_a(\rho, u) < \xi. \end{cases} \tag{2.13}$$

We summarize this information in Table 2.

	$a < -1$	$-1 < a < 0$	$0 < a$
$u_L = u > 0$	R_a to the left	R_a to the right	R_a to the left
$u_L = u < 0$	R_a to the right	R_a to the left	R_a to the right

Table 2: Existence of rarefactions of the a-family when $u_L = u_R$

2.2.2 The a-Family: $a = -1$

We now return to the special case $a = -1$. Note that the shock speed becomes

$$\begin{aligned} s_a &= u_L \left\{ 1 - \frac{\left(\rho_L \left(\frac{\rho_L}{\overline{\rho}}\right)^a - \rho \left(\frac{\rho}{\overline{\rho}}\right)^a\right)}{\rho_L - \rho} \right\} \\ &= u_L \left\{ 1 - \frac{\overline{\rho} - \overline{\rho}}{\rho_L - \rho} \right\}, \\ \implies s_a &= u_L = u. \end{aligned} \tag{2.14}$$

Since $a + 1 = 0$ when $a = -1$, we have $\lambda_a(\rho_L, u_L) = s = \lambda_a(\rho, u)$, independent of ρ_L and ρ. Thus, there is a contact discontinuity of the a-family along the line $u = u_L$.

2.2.3 Contact Discontinuities of the 0-Family: $\rho_L \neq \overline{\rho}$

We now turn to our second special assumption: that the left and right states lie on the following prescribed curve in the (ρ, u)-plane

$$\lambda_0(\rho, u) = u - u\left(\frac{\rho}{\overline{\rho}}\right)^a = u_L - u_L\left(\frac{\rho_L}{\overline{\rho}}\right)^a = \lambda_0(\rho_L, u_L). \tag{2.15}$$

This implies that the Rankine-Hugoniot jump conditions (2.8) are satisfied. Thus, it defines a contact discontinuity curve of the 0-family that is discontinuous on the line $\rho = \overline{\rho}$. We choose the branch of this C_0 that is continuous and passes through the left state, and name the other branch the "mirror" curve $C_{0,m}$, as it will be an important boundary when we analyze the regions later.

Under this assumption, we derive the curve by expressing u as a function of ρ, thus characterizing the relationship that defines the admissible states:

$$\begin{aligned} &\lambda_0(\rho, u) = \lambda_0(\rho_L, u_L), \\ \Leftrightarrow\ & u\left(1 - \left(\frac{\rho}{\overline{\rho}}\right)^a\right) = u_L - u_L\left(\frac{\rho_L}{\overline{\rho}}\right)^a, \\ \implies\ & u = \frac{1}{\overline{\rho}^a - \rho^a}\left(u_L\left(\overline{\rho}^a - \rho_L^a\right)\right), \\ \implies\ & u = \frac{1}{\overline{\rho}^a - \rho^a}\left(u_L\left(\overline{\rho}^a - \rho^a + \rho^a - \rho_L^a\right)\right), \\ \implies\ & u = \frac{\rho^a - \rho_L^a}{\overline{\rho}^a - \rho^a} u_L + u_L. \end{aligned} \tag{2.16}$$

As $\rho \to \infty$ or $\rho \to 0$, $u(\rho)$ will approach either 0 or an asymptote that will form another boundary in our region analysis. If $a > 0$,

$$\begin{aligned} \lim_{\rho \to \infty} u &= -u_L + u_L = 0, \\ \lim_{\rho \to 0} u = u(0) &= \frac{-\rho_L^a}{\overline{\rho}^a} u_L + u_L = \lambda_0(\rho_L, u_L). \end{aligned}$$

On the other hand, if $a < 0$,

$$\begin{aligned} \lim_{\rho \to \infty} u &= \frac{-\rho_L^a}{\overline{\rho}^a} u_L + u_L = \lambda_0(\rho_L, u_L), \\ \lim_{\rho \to 0} u &= -u_L + u_L = 0. \end{aligned}$$

2.2.4 The 0-Family: $\rho_L = \overline{\rho}$

We note that our previous derivation no longer applies in the case $\rho_L = \overline{\rho}$. Returning to the original criterion $\lambda_0(\rho, u) = \lambda_0(\rho_L, u_L)$ we obtain

$$u\left(1 - \left(\frac{\rho}{\overline{\rho}}\right)^a\right) = 0. \tag{2.17}$$

This implies $\rho = \overline{\rho}$ when $u \neq 0$, yielding a contact discontinuity C_0 along the line $\rho = \overline{\rho}$.

Having characterized the admissible wave patterns, we now examine whether singular solutions can be interpreted as weak solutions to the system. Our goal is to confirm that such solutions satisfy equations (1.1) and (1.2) in the distributional sense. Singular solutions are expected to arise in certain regimes, and a detailed analysis of their structure and formation will be presented in a later section.

Two principal methods are commonly used for this purpose. The first involves proposing a solution that includes Dirac delta terms and verifying its validity by inserting the expression into the weak formulation via test functions. The second approach, known as the shadow wave method, was developed by Marko Nedeljkov [6, 24, 25], and is based on constructing a sequence of smooth approximations with sharply localized internal layers that converge to the singular solution in the limit.

3 Delta-Shocks

As will be illustrated in a later section, there exist regions of the (ρ, u)-plane where there are no classical solutions nor solutions that pass through vacuum states ($\rho = 0$) or across the critical density threshold $\rho = \bar{\rho}$. This breakdown leads us to seek unbounded solutions that extend the notion of weak solutions in order to accommodate such singular behavior.

3.1 Delta-Shock and Resulting ODEs

One may justify the presence of delta-shocks by postulating a solution that includes a Dirac delta distribution and checking whether it satisfies (1.1) and (1.2) in the distributional sense.

We define a two-dimensional weighted δ-measure $\omega(s)\delta_S$ supported on a smooth curve $S = \{(x(s), t(s)) : a \leq s \leq b\}$ by

$$\langle \omega(\cdot)\delta_S, \phi(\cdot,\cdot)\rangle = \int_a^b \omega\big(t(s)\big)\phi\big(x(s), t(s)\big)\mathrm{d}s$$

for all $\phi \in C_c^\infty\big(\mathbb{R} \times (0,\infty)\big) = C_c^\infty(\mathbb{R} \times \mathbb{R}_+)$.

Motivated by numerical evidence indicating a Dirac delta concentration in ρ alone, we seek a *delta-shock type* solution of the form

$$u(x,t) = U_0(x,t), \qquad \rho(x,t) = \rho_0(x,t) + \omega(t)\delta_S(x - x(t)),$$

where

$$U_0(x,t) = \begin{cases} u_L(x,t) & x < x(t), \\ u_\delta(t) & x = x(t), \\ u_R(x,t) & x > x(t), \end{cases} \qquad \rho_0(x,t) = \begin{cases} \rho_L(x,t) & x < x(t), \\ \rho_R(x,t) & x > x(t), \end{cases}$$

where u_δ is the shock velocity, $S = \{(x(t), t) : 0 \leq t < \infty\}$, and $\omega \in C^1(\mathbb{R}_+)$. These are required to satisfy (1.1) and (1.2) in the sense of distributions, that is,

$$\langle \rho_0, \partial_t\phi\rangle + \langle f_1(\rho_0, U_0), \partial_x\phi\rangle = 0, \tag{3.1}$$
$$\langle \rho_0 U_0, \partial_t\phi\rangle + \langle f_2(\rho_0, U_0), \partial_x\phi\rangle = 0. \tag{3.2}$$

The resulting solution is interpreted in the sense of Radon measures, where the density consists of a regular part together with an atomic Dirac mass supported along the shock trajectory. In this framework

the conservation laws are satisfied at the level of measures: classical Rankine-Hugoniot relations may exhibit a deficit when considering only the left and right states, and the Dirac component accounts for the missing contribution. If a δ-shock forms in the density, then expressions involving ρ, such as ρu^n, typically inherit a singular component through multiplication by the bounded velocity field. However, these quantities do not correspond to independent conservation laws of the system. Only the variables appearing explicitly in conservative form, namely $(\rho, \rho u)$, are required to satisfy balance relations across classical or δ-shocks. This behavior is consistent with the classical theory of weak solutions: identities that rely on smooth calculus need not persist once singular waves form, and the conservation structure of the system is fully captured by the primary variables $(\rho, \rho u)$.

Note that for standard nonnegative approximations ϕ_n of the Dirac delta satisfying $\phi_n \rightharpoonup \delta$ in the distributional sense, one has $\phi_n^{a+1} \rightharpoonup 0$ whenever $a < 0$, since the exponent $a+1$ is strictly less than one. Indeed, for typical mollifiers $\phi_n(x) = nh(nx)$ with $\int_{\mathbb{R}} h(y)\,dy = 1$, one obtains $\|\phi_n\|_{L^{a+1}}^{a+1} \sim n^a \to 0$ as $n \to \infty$. Consequently, the nonlinear flux terms involving ρ_0^{a+1} do not generate additional singular contributions, and the δ-shock substitution is admissible only in the regime $a < 0$.

Let $\frac{\mathrm{d}x}{\mathrm{d}t} = u_\delta$ so that, using Green's Theorem and the compact support of ϕ,

$$
\begin{aligned}
0 &= \langle \rho_0, \partial_t \phi(x,t) \rangle + \langle f_1(\rho_0, U_0), \partial_x \phi(x,t) \rangle \\
&= \int_0^\infty \int_{-\infty}^{x(t)} \{\rho_L \partial_t \phi + f_1(\rho_L, u_L)\partial_x \phi\}\,\mathrm{d}x\mathrm{d}t \\
&\quad + \int_0^\infty \int_{x(t)}^\infty \{\rho_R \partial_t \phi + f_1(\rho_R, u_R)\partial_x \phi\}\,\mathrm{d}x\mathrm{d}t \\
&\quad + \int_0^\infty \big\{\omega(t)\partial_t \phi(x(t),t) + \omega(t) u_\delta(t) \partial_x \phi(x(t),t)\big\}\mathrm{d}t \\
&= \oint_{x(t)} -\rho_L \phi(x(t),t)\mathrm{d}x + f_1(\rho_L, u_L)\phi \mathrm{d}t \\
&\quad + \oint_{-x(t)} -\rho_R \phi(x(t),t)\mathrm{d}x + f_1(\rho_R, u_R)\phi \mathrm{d}t \\
&\quad + \int_0^\infty \omega(t)\mathrm{d}\phi \\
&= \int_0^\infty -\{\rho_L - \rho_R\}\,\phi(x(t),t)x'(t)\mathrm{d}t \\
&\quad + \int_0^\infty \{f_1(\rho_L, u_L) - f_1(\rho_R, u_R)\}\,\phi(x(t),t)\mathrm{d}t \\
&\quad + \phi(x(t),t)\omega(t)\Big|_0^\infty - \int_0^\infty \phi(x(t),t)\frac{\mathrm{d}}{\mathrm{d}t}\big(\omega(t)\big)\mathrm{d}t, \\
\implies & -[\rho]x'(t) + [f_1(\rho,u)] = \frac{\mathrm{d}}{\mathrm{d}t}\big(\omega(t)\big).
\end{aligned}
$$

Using similar calculations on (3.2), we obtain the following result:

$$
-[\rho u]x'(t) + [f_2(\rho,u)] = \frac{\mathrm{d}}{\mathrm{d}t}\big(\omega(t)u_\delta(t)\big).
$$

We impose the initial conditions $x(0) = 0, \omega(0) = 0,$ and $u_\delta(0) = s_- \in \mathbb{R}$. Thus, we have

$$
\frac{\mathrm{d}x}{\mathrm{d}t} = u_\delta(t), \tag{3.3}
$$

$$
\frac{\mathrm{d}}{\mathrm{d}t}\big(\omega(t)u_\delta(t)\big) = -[\rho u]x'(t) + \left[\rho u^2 - \rho u^2 \left(\frac{\rho}{\overline{\rho}}\right)^a\right], \tag{3.4}
$$

$$
\frac{\mathrm{d}}{\mathrm{d}t}\big(\omega(t)\big) = -[\rho]x'(t) + \left[\rho u - \rho u \left(\frac{\rho}{\overline{\rho}}\right)^a\right]. \tag{3.5}
$$

This system corresponds exactly to the shadow wave method (discussed in the following section) where $u_\delta(t) = \eta_0(t) = \eta_1(t)$ and $\omega(t) = \zeta_0(t) + \zeta_1(t)$. Using this connection, we can determine the value of $u_\delta(0) = s_-$ in both cases, as we do at the end of Section 3.2.1.

3.2 Nedeljkov's Shadow Wave Method for Singular and Delta-Shocks

Following [6, 24, 25], consider the following weighted shadow wave solution to the equations (1.1) and (1.2),

$$(\rho_\varepsilon, u_\varepsilon) = \begin{cases} (\rho_L, u_L) & x < x(t) - \varepsilon, \\ (\rho_{L,\varepsilon}(t), u_{L,\varepsilon}(t)) & x(t) - \varepsilon < x < x(t), \\ (\rho_{R,\varepsilon}(t), u_{R,\varepsilon}(t)) & x(t) < x < x(t) + \varepsilon, \\ (\rho_R, u_R) & x(t) + \varepsilon < x, \end{cases} \tag{3.6}$$

for $\varepsilon > 0, x(t) \in C^1\big([0,\infty)\big)$.

We expect an unbounded solution in at least one of the two dependent variables, connecting the left state (ρ_L, u_L) to the right state (ρ_R, u_R), while allowing the amplitude to vary across the discontinuity and evolve in time. Thus, we have the piecewise function

$$\begin{aligned} \rho_\varepsilon(x,t) = &\{1 - H(x - x(t) + \varepsilon)\}\,\rho_L \\ &+ \{H(x - x(t) + \varepsilon) - H(x - x(t))\}\,\rho_{L,\varepsilon}(t) \\ &+ \{H(x - x(t)) - H(x - x(t) - \varepsilon)\}\,\rho_{R,\varepsilon}(t) \\ &+ H(x - x(t) - \varepsilon)\rho_R, \end{aligned}$$

and the equation for u_ε is similar. Let

$$\rho_{L,\varepsilon}(t) = \frac{\zeta_L(t)}{\varepsilon^k}, \rho_{R,\varepsilon}(t) = \frac{\zeta_R(t)}{\varepsilon^\beta}, u_{L,\varepsilon}(t) = \frac{\eta_L(t)}{\varepsilon^\gamma}, u_{R,\varepsilon}(t) = \frac{\eta_R(t)}{\varepsilon^\delta}, \tag{3.7}$$

where k, β, γ, δ will be chosen later such that a solution is admitted. H is the Heaviside step function. Thus, we have

$$\begin{aligned} \partial_t \rho_\varepsilon = &\delta(x - x(t) + \varepsilon)x'(t)\rho_L \\ &- \delta(x - x(t) + \varepsilon)x'(t)\rho_{L,\varepsilon}(t) + \delta(x - x(t))x'(t)\rho_{L,\varepsilon}(t) \\ &+ \{H(x - x(t) + \varepsilon) - H(x - x(t))\}\,\rho'_{L,\varepsilon}(t) \\ &- \delta(x - x(t))x'(t)\rho_{R,\varepsilon}(t) + \delta(x - x(t) - \varepsilon)x'(t)\rho_{R,\varepsilon}(t) \\ &+ \{H(x - x(t)) - H(x - x(t) - \varepsilon)\}\,\rho'_{R,\varepsilon}(t) \\ &- \delta(x - x(t) - \varepsilon)x'(t)\rho_R. \end{aligned}$$

For a test function $\phi \in C_c^\infty(\mathbb{R} \times \mathbb{R}_+)$,

$$\begin{aligned} \langle \partial_t \rho_\varepsilon, \phi \rangle &= \iint_{\mathbb{R}^2_+} \partial_t \rho_\varepsilon(x,t) \cdot \phi(x,t)\mathrm{d}x\mathrm{d}t \\ &= \int_0^\infty \{\rho_L x'(t)\phi(x(t) - \varepsilon, t) - \rho_{L,\varepsilon}(t)x'(t)\phi(x(t) - \varepsilon, t) \\ &\quad + \rho_{L,\varepsilon}(t)x'(t)\phi(x(t), t) - \rho_{R,\varepsilon}(t)x'(t)\phi(x(t), t) \\ &\quad + \rho_{R,\varepsilon}(t)x'(t)\phi(x(t) + \varepsilon) - \rho_R x'(t)\phi(x(t) + \varepsilon, t)\}\mathrm{d}t \\ &\quad + \int_0^\infty \int_{x(t)-\varepsilon}^{x(t)} \rho'_{L,\varepsilon}(t)\phi(x,t)\mathrm{d}x\mathrm{d}t \\ &\quad + \int_0^\infty \int_{x(t)}^{x(t)+\varepsilon} \rho'_{R,\varepsilon}(t)\phi(x,t)\mathrm{d}x\mathrm{d}t. \end{aligned}$$

Using the approximation $\phi(x \pm \varepsilon, t) = \phi(x,t) \pm \varepsilon \partial_x \phi(x,t) + \mathcal{O}(\varepsilon^2)$ and the Mean Value Theorem for $\int_{x(t)}^{x(t)+\varepsilon} \phi(x,t)\mathrm{d}x$, we obtain

$$\begin{aligned}
\langle \partial_t \rho_\varepsilon, \phi \rangle &\approx \int_0^\infty \left\{ x'(t)(\rho_L - \rho_R) + \varepsilon(\rho'_{L,\varepsilon}(t) + \rho'_{R,\varepsilon}(t)) \right\} \phi(x(t),t)\mathrm{d}t \\
&\quad + \int_0^\infty \left\{ \varepsilon x'(t)(\rho_{L,\varepsilon}(t) - \rho_L + \rho_{R,\varepsilon}(t) - \rho_R) \right\} \partial_x \phi(x(t),t)\mathrm{d}t \\
&= \left\langle \left(x'(t)(\rho_L - \rho_R) + \varepsilon(\rho'_{L,\varepsilon} + \rho'_{R,\varepsilon}) \right) \delta(x - x(t)), \phi(x,t) \right\rangle \\
&\quad + \left\langle -\varepsilon x'(t)(\rho_{L,\varepsilon} - \rho_L + \rho_{R,\varepsilon} - \rho_R)\delta'(x - x(t)), \phi(x,t) \right\rangle .
\end{aligned}$$

Note that $f \approx g$ means that $\frac{f-g}{\varepsilon}$ converges to zero as $\varepsilon \to 0$. We continue with the flux:

$$\begin{aligned}
&\left\langle \partial_x \left(\rho_\varepsilon u_\varepsilon \left(1 - \left(\frac{\rho}{\overline{\rho}} \right)^a \right) \right), \phi(x,t) \right\rangle \\
&= - \left\langle \rho_\varepsilon u_\varepsilon \left(1 - \left(\frac{\rho}{\overline{\rho}} \right)^a \right), \partial_x \phi(x,t) \right\rangle \\
&= - \int_0^\infty \int_{-\infty}^{x(t)-\varepsilon} \rho_L u_L \left(1 - \left(\frac{\rho_L}{\overline{\rho}} \right)^a \right) \partial_x \phi \mathrm{d}x\mathrm{d}t \\
&\quad - \int_0^\infty \int_{x(t)-\varepsilon}^{x(t)} \rho_{L,\varepsilon} u_{L,\varepsilon} \left(1 - \left(\frac{\rho_{L,\varepsilon}}{\overline{\rho}} \right)^a \right) \partial_x \phi \mathrm{d}x\mathrm{d}t \\
&\quad - \int_0^\infty \int_{x(t)}^{x(t)+\varepsilon} \rho_{R,\varepsilon} u_{R,\varepsilon} \left(1 - \left(\frac{\rho_{R,\varepsilon}}{\overline{\rho}} \right)^a \right) \partial_x \phi \mathrm{d}x\mathrm{d}t \\
&\quad - \int_0^\infty \int_{x(t)+\varepsilon}^{\infty} \rho_R u_R \left(1 - \left(\frac{\rho_R}{\overline{\rho}} \right)^a \right) \partial_x \phi \mathrm{d}x\mathrm{d}t \\
&\approx \int_0^\infty -f_1(\rho_L, u_L)\big(\phi(x(t),t) - \varepsilon \partial_x \phi(x(t),t)\big) + f_1(\rho_{L,\varepsilon}, u_{L,\varepsilon})\big(\phi(x(t),t) - \varepsilon \partial_x \phi(x(t),t)\big) \\
&\qquad - f_1(\rho_{L,\varepsilon}, u_{L,\varepsilon})\phi(x(t),t) + f_1(\rho_{R,\varepsilon}, u_{R,\varepsilon})\phi(x(t),t) \\
&\qquad - f_1(\rho_{R,\varepsilon}, u_{R,\varepsilon})\big(\phi(x(t),t) + \varepsilon \partial_x \phi(x(t),t)\big) + f_1(\rho_R, u_R)\big(\phi(x(t),t) + \varepsilon \partial_x \phi(x(t),t)\big)\mathrm{d}t \\
&= \langle - \left\{ f_1(\rho_L, u_L) - f_1(\rho_R, u_R) \right\} \delta(x - x(t)), \phi(x,t) \rangle \\
&\quad + \langle \varepsilon \left\{ f_1(\rho_{L,\varepsilon}, u_{L,\varepsilon}) - f_1(\rho_L, u_L) + f_1(\rho_{R,\varepsilon}, u_{R,\varepsilon}) - f_1(\rho_R, u_R) \right\} \delta'(x - x(t)), \phi(x,t) \rangle .
\end{aligned}$$

Since the sum of these two terms must equal 0 for all $\varepsilon > 0$ according to (1.1), we require

$$x'(t)[\rho] + \lim_{\varepsilon \to 0} \left\{ \varepsilon \rho'_{L,\varepsilon}(t) + \varepsilon \rho'_{R,\varepsilon}(t) \right\} - [f_1(\rho, u)] = 0, \tag{3.8}$$

$$-x'(t) \lim_{\varepsilon \to 0} \left\{ \varepsilon \rho_{L,\varepsilon}(t) + \varepsilon \rho_{R,\varepsilon}(t) \right\} + \lim_{\varepsilon \to 0} \left\{ \varepsilon f_1\big(\rho_{L,\varepsilon}(t), u_{L,\varepsilon}(t)\big) + \varepsilon f_1\big(\rho_{R,\varepsilon}(t), u_{R,\varepsilon}(t)\big) \right\} = 0. \tag{3.9}$$

Using similar calculations for $\langle \partial_t(\rho u), \phi \rangle$ and $\langle \partial_x(f_2(\rho,u)), \phi \rangle$, we obtain

$$x'(t)[\rho u] + \lim_{\varepsilon \to 0} \left\{ \varepsilon(\rho_{L,\varepsilon} u_{L,\varepsilon})'(t) + \varepsilon(\rho_{R,\varepsilon} u_{R,\varepsilon})'(t) \right\} - [f_2(\rho, u)] = 0, \tag{3.10}$$

$$-x'(t) \lim_{\varepsilon \to 0} \left\{ \varepsilon(\rho_{L,\varepsilon} u_{L,\varepsilon})(t) + \varepsilon(\rho_{R,\varepsilon} u_{R,\varepsilon})(t) \right\} + \lim_{\varepsilon \to 0} \left\{ \varepsilon f_2\big(\rho_{L,\varepsilon}(t), u_{L,\varepsilon}(t)\big) + \varepsilon f_2\big(\rho_{R,\varepsilon}(t), u_{R,\varepsilon}(t)\big) \right\} = 0. \tag{3.11}$$

Thus, (1.1) and (1.2) are satisfied by the shadow wave ansatz (3.6) if and only if (3.8) - (3.11) hold. We now seek to determine values of the parameters k, β, γ, δ such that each of the limits is finite, thereby ensuring that the equations are satisfied.

3.2.1 Delta Solutions for $a < 0$

For $a < 0$, there are many combinations of exponents which yield a solution to (3.8) - (3.11), but the one we observe numerically (see [5]) is described here. It is also the same as that produced by the previous method for delta-shocks examined in Section 3.1.

Let $k = \beta = 1$ and $\gamma = \delta = 0$. Using (3.7), $\kappa_1(t) = x'(t)[\rho] - [f_1(\rho, u)]$, and $\kappa_2(t) = x'(t)[\rho u] - [f_2(\rho, u)]$, (3.8) - (3.11) become

$$\begin{aligned}
-\kappa_1(t) &= \zeta_L'(t) + \zeta_R'(t),\\
x'(t)\big(\zeta_L(t) + \zeta_R(t)\big) &= \zeta_L\eta_L(t) + \zeta_R(t)\eta_R(t),\\
-\kappa_2(t) &= (\zeta_L\eta_L)'(t) + (\zeta_R\eta_R)'(t),\\
x'(t)\big((\zeta_L\eta_L)(t) + (\zeta_R\eta_R)(t)\big) &= (\zeta_L\eta_L)(t)\eta_L(t) + (\zeta_R\eta_R)(t)\eta_R(t).
\end{aligned}$$

Let $\zeta(t) := \zeta_L(t) + \zeta_R(t)$ and $\eta(t) = \eta_L(t) = \eta_R(t)$, so we obtain

$$x'(t) = \eta(t), \tag{3.12}$$
$$\zeta'(t) = -\kappa_1(t), \tag{3.13}$$
$$(\zeta\eta)'(t) = -\kappa_2(t). \tag{3.14}$$

This system corresponds exactly to the one obtained using the method proposed in Section 3.1.

Note that the initial value problem specified in (1.4) also provides the initial conditions for the present system. Because the unbounded behavior is anticipated at the discontinuity, we set $x(0) = 0$. Additionally, the initial conditions are bounded, which requires $\zeta(0) = 0$. Finally, observe that $x'(t) = \eta(t) \equiv \frac{\kappa_2(t)}{\kappa_1(t)} \equiv \frac{\kappa_2(0)}{\kappa_1(0)}$ solves the system of ODEs. This corresponds to the solutions we numerically observed in [5] where $\zeta(t)$ grows linearly over time. Assuming a continuous $\eta(t)$, let us determine the form of $s_- = x'(0)$: let $K_1(t) = \int_0^t \kappa_1(s)\mathrm{d}s$ and $K_2(t) = \int_0^t \kappa_2(s)\mathrm{d}s$. Then

$$\begin{aligned}
\zeta(t) &= -K_1(t) = -x(t)[\rho] + [f_1(\rho, u)]t,\\
\zeta(t)\eta(t) &= -K_2(t) = -x(t)[\rho u] + [f_2(\rho, u)]t,\\
\implies x'(0) = s_- &= \lim_{\varepsilon\to 0} \frac{\zeta(\varepsilon)\eta(\varepsilon)}{\zeta(\varepsilon)} = \lim_{\varepsilon\to 0} \frac{-K_2(\varepsilon)}{-K_1(\varepsilon)}\\
&= \lim_{\varepsilon\to 0} \frac{x'(\varepsilon)[\rho u] - [f_2(\rho, u)]}{x'(\varepsilon)[\rho] - [f_1(\rho, u)]}\\
&= \frac{s_-[\rho u] - \left[\rho u^2\left(1 - \left(\frac{\rho}{\overline{\rho}}\right)^a\right)\right]}{s_-[\rho] - \left[\rho u\left(1 - \left(\frac{\rho}{\overline{\rho}}\right)^a\right)\right]},\\
\implies s_-^2[\rho] - s_-&\left([\rho u] + \left[\rho u\left(1 - \left(\frac{\rho}{\overline{\rho}}\right)^a\right)\right]\right) + \left[\rho u^2\left(1 - \left(\frac{\rho}{\overline{\rho}}\right)^a\right)\right] = 0.
\end{aligned} \tag{3.15}$$

3.2.2 Delta Solutions for $a > 0$

For $a > 0$, we can also identify multiple combinations that could yield admissible solutions. However, the configuration observed in our numerical simulations satisfies the Rankine–Hugoniot condition only in the second component of (2.8) while a deficit remains in the first component; that is, $\kappa_1(t) \not\equiv 0 \equiv \kappa_2(t)$. Furthermore, numerical evidence indicates that the delta concentration in ρ occurs when $u = 0$, suggesting that $\lim_{\varepsilon\to 0} u_{i,\varepsilon} = 0$.

Let $k = \beta = 1$, $\gamma = \delta = -a$. Then (3.8) - (3.11) become

$$\begin{aligned}
-\kappa_1(t) &= \zeta_L'(t) + \zeta_R'(t),\\
-x'(t)\big(\zeta_L(t) + \zeta_R(t)\big) &= \zeta_L(t)\eta_L(t)\left(\frac{\zeta_L(t)}{\overline{\rho}}\right)^a + \zeta_R(t)\eta_R(t)\left(\frac{\zeta_R(t)}{\overline{\rho}}\right)^a,\\
\kappa_2(t) = 0 &\Leftrightarrow x'(t) = \frac{[f_2(\rho, u)]}{[\rho u]},\\
0 &= 0.
\end{aligned}$$

Note now that $[\rho u] \neq 0$ outside of the regions in which we can connect the left and right states with combinations of classical curves. Let $\zeta(t) := \zeta_L(t) + \zeta_R(t)$ and $\eta(t) = \eta_L(t) = \eta_R(t)$ so that we obtain

$$x'(t) \equiv s_+ = \frac{[f_2(\rho, u)]}{[\rho u]}, \tag{3.16}$$

$$\zeta'(t) = -\kappa_1 = -s_+[\rho] + [f_1(\rho, u)], \tag{3.17}$$

$$\eta(t) = -s_+ \left(\frac{\overline{\rho}}{\frac{1}{2}\zeta(t)} \right)^a. \tag{3.18}$$

As we are still working within the framework of the Riemann problem, we impose the same type of initial conditions as in the previous case, namely, $\zeta(0) = 0$ and $x(0) = 0$.

Our solution to (3.6), therefore, in the limit $\varepsilon \to 0$ is of the form

$$u(x,t) = \begin{cases} u_L & x < x(t), \\ 0 & x = x(t), \\ u_R & x > x(t), \end{cases} \qquad \rho(x,t) = \begin{cases} \rho_L & x < x(t), \\ \left(-\frac{[f_2(\rho,u)]}{[\rho u]}[\rho] + [f_1(\rho,u)] \right) t \cdot \delta\big(x - x(t)\big) & x = x(t), \\ \rho_R & x > x(t). \end{cases}$$

We seek delta-shocks connecting a given left state (ρ_L, u_L) with a right state (ρ_R, u_R) that are overcompressive, meaning that all characteristic curves run into the delta-shock curve from both sides. Therefore, we use the following inequality as our admissibility criterion

$$\max\{\lambda_a(U_R), \lambda_0(U_R)\} < s_\pm < \min\{\lambda_a(U_L), \lambda_0(U_L)\}. \tag{3.19}$$

We can now compare the initial speed $x'(0) = s_\pm$ with our overcompressive admissibility condition (3.19) and determine where delta-shock solutions are expected (see Figure 1). We also note that reducing (3.3) - (3.5) to solving for $u_\delta(t)$ yields a nonlinear second-order ODE which cannot be solved analytically. Although other solution profiles may exist, our numerical experiments consistently yield the constant-speed solution described above.

In the following section, we present plots for various values of a, highlighting the resulting wave structures and their dependence on the system's parameters.

4 Regions of Classical and Nonclassical Solutions: 24 Cases

4.1 Numerical Preliminaries

For completeness we summarize here the main features of the numerical procedure and the resulting solution profiles. Detailed graphical illustrations of the simulations have been presented in our companion work by Culver et al. [5], to which we refer the reader for representative figures and further discussion. Since the present paper focuses on the analytical structure of the solutions and the measure-valued formulation of the δ-shock, we do not reproduce those figures here in order to avoid duplication of material.

The Local Lax-Friedrichs (LLF) scheme is a well-known numerical approximation that is used to reconstruct the flux of hyperbolic conservation laws. In essence, the scheme begins with a discretization of the spatial and temporal domains into a mesh grid, after which the solution is numerically approximated at each mesh point in fixed time. By letting Δx and Δt be the corresponding cell sizes, we can write any point in our grid as $(x_i, t_j) = (i\Delta x, j\Delta t)$, and the solution $H = (\rho \ \rho u)^T$ can be written similarly at any point as $H_i^j = H(x_i, t_j)$. To find the solution H at the point (x_i, t_{j+1}), one only needs to have constructed the values at (x_{i-1}, t_j) and (x_{j+1}, t_j). The relevant flux reconstruction is given by the equation:

$$H_i^{j+1} = \frac{1}{2}(H_{i-1}^j + H_{i+1}^j) + \frac{CFL}{2\lambda}(G_{i+1}^j - G_{i-1}^j) \tag{4.1}$$

where $CFL = \lambda \frac{\Delta t}{\Delta x}$ is the Courant number and $\lambda := \max_i |\lambda_i|$ is the greater of the two characteristic speeds. The Courant number measures the numerical stability of the scheme and must satisfy the inequality

$$CFL \leq \frac{1}{2}. \tag{4.2}$$

By choosing $\Delta x = 1$, this can be ensured by simply requiring $\lambda \Delta t \leq \frac{1}{2}$ throughout the procedure. Thus, our spatial grid size is always fixed, but our temporal steps may differ greatly depending on the eigenvalues calculated at each iteration. The CFL condition guarantees that the scheme converges to the physically correct weak solution satisfying the Lax Entropy Condition [30]. Additionally, for a more in-depth treatment and explanation of the LLF scheme, consult [17, 18].

Because the system's eigenvalues can greatly influence the values of Δt, certain choices of physical parameters prove easier to analyze numerically than others. The problem can be simplified into a multitude of cases depending on the system parameters and initial states. For our simulation, we chose the following conditions:

- $\overline{\rho} = 5$;
- $a \in \{-1.5, -1, -0.5, 0.5\}$ for each of the four cases of a we will consider;
- $\rho_L \in \{3, 5, 8\}$ and $u_L = \pm 4$, depending on the ordering ρ_L and $\overline{\rho}$ and the sign of u_L.

Note that we have introduced the change of variables in our code $m = \rho u$ so that our solution vector may be written more simply as $H = (\rho \;\; m)^T$. Furthermore, our left and right states are represented in our figures as $L = (\rho_L \;\; u_L)^T$ and $R = (\rho \;\; u)^T$, respectively. Lastly, to ensure accuracy, data was renormalized every 100 steps within an error bound of 10^{-7} to minimize numerical noise.

4.2 Interpretation of Numerical Outputs

Because our solution is self-similar when there is no time-dependence in the flux functions (see Culver et al. [5] for a treatment of the system with a time-dependent source term), we can express the solution in terms of x/t. When interpreting the numerical figures, we look at the graphs of ρ and u against x/t together and compare how ρ and u change or remain constant at the same x/t values. Our original plots showed 20 iterations (each with 1000 steps) to illustrate behavior over time, while the right column displayed the final iteration, the iteration most closely portraying the weak solution. We used an increasing thickness to differentiate the graphs at different times. A single graph may show multiple features in sequence, such as an R_a followed by a vacuum and then a C_0. We expect the following behaviors from our analysis in Sections 2 and 3:

- If ρ changes (increasing or decreasing) while u remains constant:
  - For $a \neq -1$, this indicates an S_a, a shock of the a-family or a-shock, or an R_a, an a-rarefaction:
    - If ρ changes abruptly, there is a jump discontinuity and thus an a-shock.
    - If ρ changes continuously, there is an R_a.
  - For $a = -1$, this indicates a C_a, an a-contact discontinuity.
- If $\rho_L \neq \overline{\rho}$, then ρ and u changing simultaneously indicates a C_0. However, if $\rho_L = \overline{\rho}$, then C_0 appears as a vertical line, where $\rho = \rho_L = \overline{\rho}$ remains constant while u changes.
- If ρ reaches zero, this is called a vacuum state.
- If u is changing by a small amount, but ρ spikes to a large value (resembling a Dirac delta), this indicates a delta-shock.

4.3 Discussion of Regions

The equations for our shocks, rarefactions, and contact discontinuities are given by

$$S(\rho_L, u_L) : u = u_L, \tag{4.3}$$

$$R(\rho_L, u_L) : u = u_L, \tag{4.4}$$

$$C(\rho_L, u_L) : u = u_L \left(\frac{\rho^a - \rho_L^a}{\overline{\rho}^a - \rho^a} + 1 \right). \tag{4.5}$$

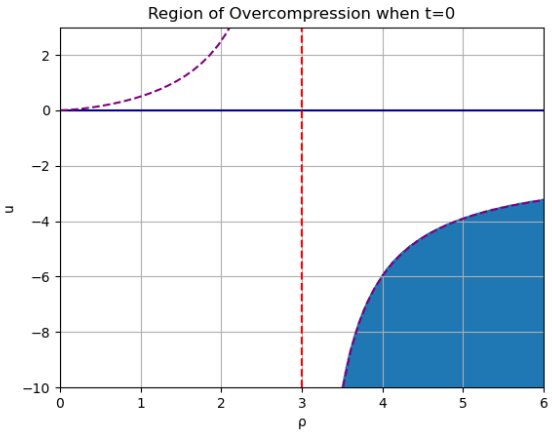

Figure 1: Overcompressive Region for Case 4

The regions are further defined by the ρ-axis and the max bound of the overcompressive region calculated numerically in Python following the shadow wave method. Take Case 4 (which will be described in greater depth later on) as an example where $C_{0,m}$ bounds the region where delta-shock solutions occur, marked by the shaded area. We will find that it is often the case that these overcompressive regions are bounded by $C_{0,m}$ and by the ρ-axis on occasion. Some limiting behavior of $C(\rho, u)$ as $\rho \to 0$ or ∞ also occurs and separates regions of solutions, including the asymptotes discussed at the end of Section 2.2.3 and, when $a < 0$, $C_{0,\ell}$ the limiting contact discontinuity at $\rho_L \to \infty$, given by the equation

$$C_{0,\ell}(\rho_L, u_L) : u = u_L \left(\frac{-\rho^a}{\overline{\rho}^a - \rho^a} + 1 \right). \tag{4.6}$$

Recall the formulation of the Riemann problem in equation (1.4). We have a left state (ρ_L, u_L) and a right state (ρ, u), and we seek a solution path between them in state space. For any given case, we can split the state space into regions of different solutions and analyze them accordingly. Of our twenty-four cases, we observe a total of six types of regions, each displaying a characteristic wave or combination of waves. Listed here, they are

- Region I: S_a and C_0
  The solution to the Riemann problem in this region is classical. The left state is connected to the right by means of a shock and contact discontinuity, the order of which depends on the case being considered.

- Region II: R_a and C_0
  The transition from the left state to the right state occurs via a rarefaction wave followed by a contact discontinuity. The rarefaction continuously connects states that do not satisfy the Lax Entropy Condition, as the characteristic speed increases across the wave. The order of the waves is again dependent on the eigenvalues in the specific case.

- Region III: C_a and C_0
  When $a = -1$, the shock and rarefactions of the a-family become a single contact discontinuity along the line $u = u_L$. The order of the two contact discontinuities depends on whether $u_L > 0$ or not.

- Region IV: Delta-Shock S_δ
  The right state exists in a region that cannot be reached by classical means. The solution becomes unbounded in the ρ variable when the left and right states satisfy the overcompressibility condition. There may also be curves of the a-family which supplement the delta-shock. A lack of subscript will denote regions where only a delta-shock connects the left and right states.

- Region V: Vacuum
  The right state can only be reached by allowing the density of the system to hit zero, creating a vacuum state. In some of the figures that follow, the vacuum state may be divided into subregions based on the waves that combine to produce the solution. This will be denoted by the subscript for the region: for instance, "Region $V_{C_0VC_aC_0}$" refers to a contact discontinuity into a vacuum followed by two more contact discontinuities. In this example, two contact discontinuities of the same 0-family are allowed because we pass through the degeneracy $\rho = 0$.

- Region VI: States that pass through degeneracy
  When $u = 0$, the system loses hyperbolicity and we have to "reset" the Riemann problem. Thus, we are able to employ two classical curves of the same family on either side of the degeneracy, which will arise as a curve of the a-family followed by a C_0 along the line $\rho = \overline{\rho}$ (when $\lambda_0 = 0$) and finishing with another curve of the a-family.

Note that in the region descriptions throughout this paper, the subscript indicates which wave family appears first in the path. For example, I_a means that in the region I, the left state first connects to the middle state via the a-family curve, specifically through a shock S_a, followed by a contact discontinuity C_0.

4.3.1 $a < -1$

We consider first

- Case 1: $u_L < 0$ and $\rho_L < \overline{\rho}$,
- Case 2: $u_L < 0$ and $\rho_L = \overline{\rho}$, and
- Case 3: $u_L < 0$ and $\rho_L > \overline{\rho}$,

and we discuss the various regions and the types of wave combinations that comprise the solution to the Riemann Problem, detailing the path taken to reach the right state.

For Cases 1 - 3, we have the following regions:

- Region I_a: The left state is connected to the right by an a-shock followed by a 0-contact discontinuity.
- Region II_a: The left state is connected to the right by an a-rarefaction curve followed by a 0-contact discontinuity.
- Region IV_a: The left state is connected to the right state via an a-rarefaction to a middle state, followed by an overcompressive δ-shock.
- Region VI: The left state will either take an R_a or S_a, in Cases 1 and 3, respectively, to reach $\overline{\rho}$, unless the left state is already at $\overline{\rho}$ to begin with. Then it will go up $\rho = \overline{\rho}$ using the C_0 curve of Case 2. Finally, it will then take either an S_a or an R_a from $(\overline{\rho}, u)$ to reach the right state (ρ, u) as in Case 5 (presented shortly).

As shown above, the solution to the Riemann problem will involve multiple different cases (as we use the word) for the various middle states as the values of ρ and u evolve. For instance, suppose we have chosen our initial conditions so that we are in Case 1 with $\rho > \overline{\rho}$ and $u < 0$. We then have that the solution will follow the rarefaction curve R_a into Case 3 before following the contact discontinuity C_0. We have carefully chosen the numbering of our regions so that a right state, say, in Region I_a is always achieved in the manner of $S_a \to C_0$. In Figure 2, we present the state spaces for Cases 1 - 3:

We then turn to the remaining three regions of (ρ_L, u_L):

- Case 4: $u_L > 0$ and $\rho_L < \overline{\rho}$,
- Case 5: $u_L > 0$ and $\rho_L = \overline{\rho}$, and
- Case 6: $u_L > 0$ and $\rho_L > \overline{\rho}$.

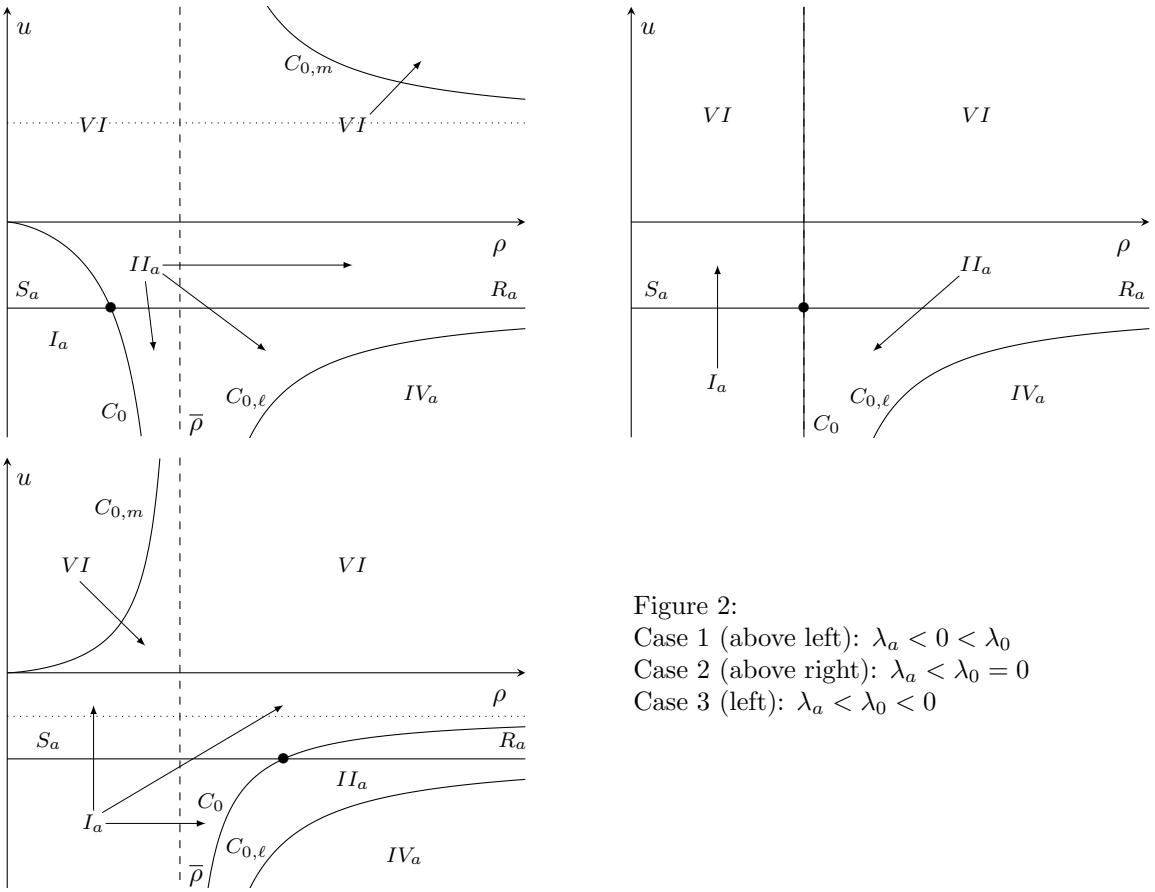

Figure 2:
Case 1 (above left): $\lambda_a < 0 < \lambda_0$
Case 2 (above right): $\lambda_a < \lambda_0 = 0$
Case 3 (left): $\lambda_a < \lambda_0 < 0$

These are comparable to Cases 1, 2, and 3 except that $u_L > 0$. In addition, a vacuum region exists in these cases where ρ hits zero. The regions for the solution to the Riemann problem are as follows:

- Regions I_0, II_0, and IV: The same wave connections as in Cases 1 - 3, but the sequence in which these waves occur is reversed. That is, in Region I_0, the left state is connected to the right in the manner of $C_0 + S_a$, instead of $S_a + C_0$.
  - Region IV_δ: The left state first follows an over-compressive δ-shock S_δ. It then follows an a-rarefaction to the right state.
- Region V: This occurs when the path from the left state to the right state passes through a vacuum state. In cases where a vacuum arises, the path between states often involves a sequence of waves. The following are typical wave sequences that occur when a vacuum is present:
  - $V_{C_0VC_0}$: The solution consists of a C_0 from the left state to a vacuum, followed by another C_0 from the vacuum to the right state as in Case 1.
  - $V_{C_0VR_aC_0}$: The solution consists of a C_0 from the left state to a vacuum. It then goes from the vacuum to an R_a, followed by another C_0 as in Case 1, going to Case 3.
  - $V_{R_aVC_0}$ - The solution consists of an R_a from the left state to a vacuum. It then goes from the vacuum to a C_0 as in Case 1.

Below, we present the state spaces for Cases 4 through 6:

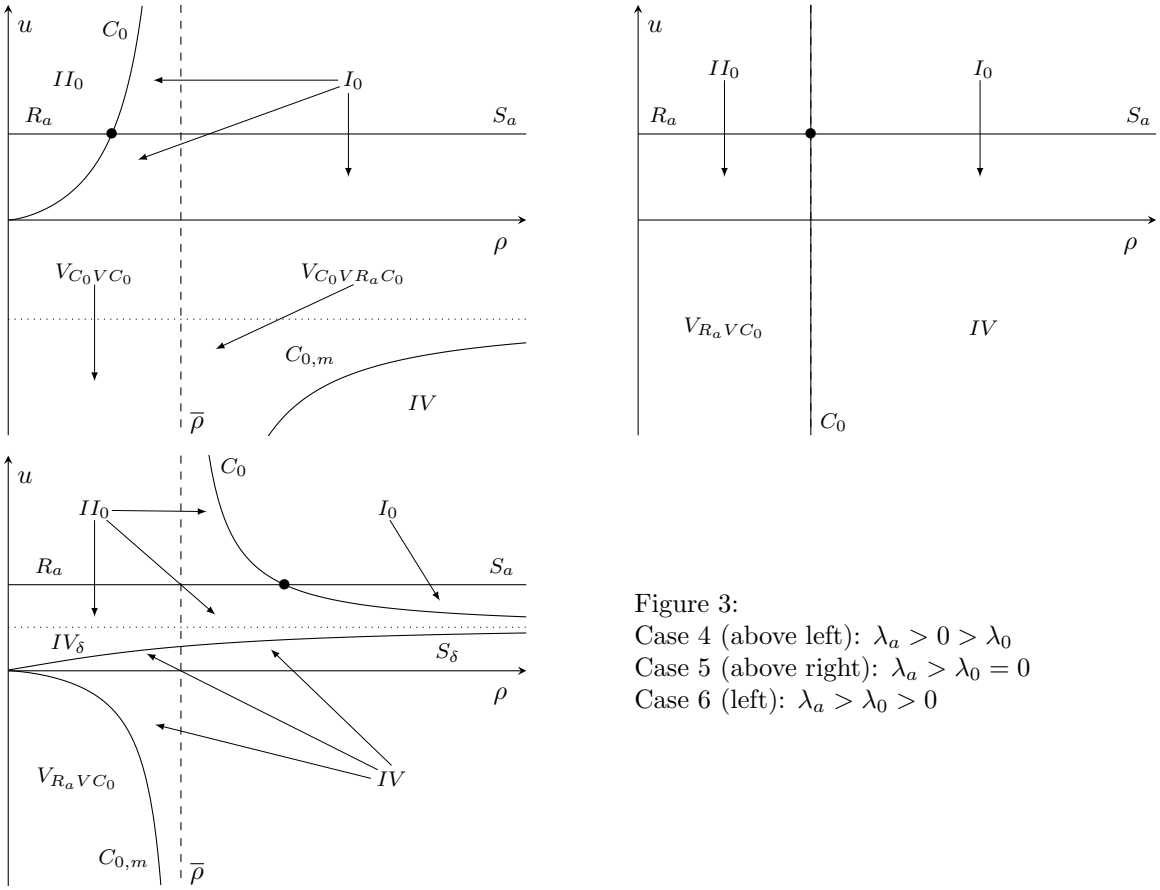

Figure 3:
Case 4 (above left): $\lambda_a > 0 > \lambda_0$
Case 5 (above right): $\lambda_a > \lambda_0 = 0$
Case 6 (left): $\lambda_a > \lambda_0 > 0$

4.3.2 $-1 < a < 0$

We note that the structure of the $-1 < a < 0$ cases are similar to the structure of the $a < -1$ cases. The only difference is that the portions of the line $u = u_L$ have now reversed roles from S_a to R_a and vice versa. We identify three more cases:

- Case 13: $u_L < 0$ and $\rho_L < \overline{\rho}$,
- Case 14: $u_L < 0$ and $\rho_L = \overline{\rho}$, and
- Case 15: $u_L < 0$ and $\rho_L > \overline{\rho}$.

We now discuss the solutions to the Riemann Problems in the various regions and detail the path that is taken to reach the right state. For Cases 13 - 15, we have the following regions:

- Region I_a: The left state is connected to the right by an a-shock followed by a 0-contact discontinuity.
- Region II_a: The left state is connected to the right state by a rarefaction curve R_a followed by a C_0.
- Region IV: The left state follows an overcompressive delta-shock S_δ as ρ blows up.
- Region VI: The left state will either take an a-shock or rarefaction curve to first reach $\overline{\rho}$, from Case 13 and Case 15, respectively, going into Case 14. It will then travel along $\overline{\rho}$ via a 0-contact discontinuity, finishing with an a-shock or a-rarefaction curve to the right state.

Below, we present the state spaces for Cases 13 through 15.

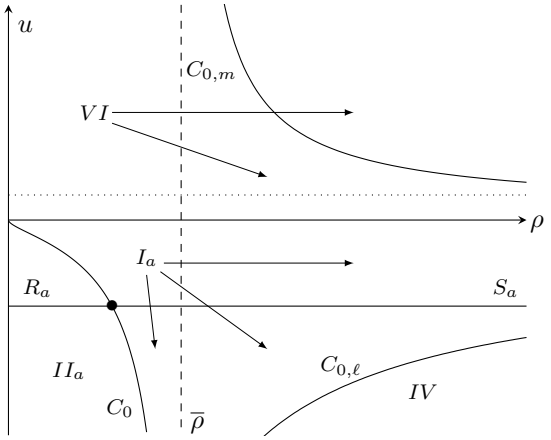

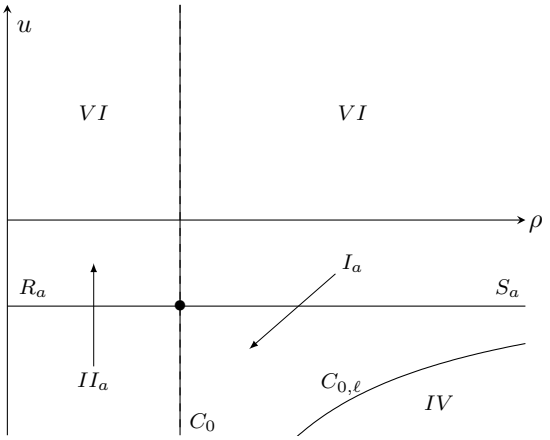

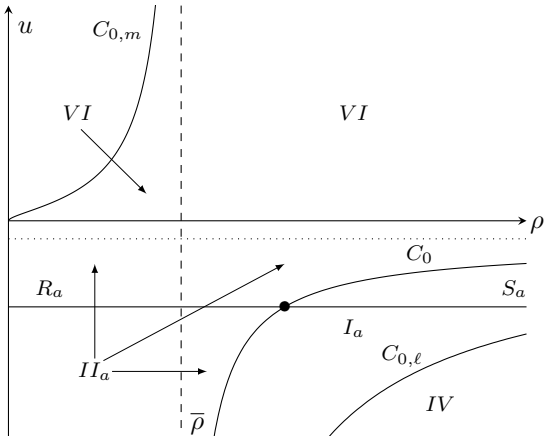

Figure 4:
Case 13 (above left): $\lambda_a < \lambda_0$ and $0 < \lambda_0$
Case 14 (above right): $\lambda_a < \lambda_0 = 0$
Case 15 (left): $\lambda_a < \lambda_0 < 0$

Cases 16 - 18 are similar:

- Case 16: $u_L > 0$ and $\rho_L < \overline{\rho}$,
- Case 17: $u_L > 0$ and $\rho_L = \overline{\rho}$, and
- Case 18: $u_L > 0$ and $\rho_L > \overline{\rho}$.

These are the versions of Cases 13, 14, and 15 where $u_L > 0$. Additionally, a vacuum region exists in these cases where ρ hits zero. The regions for the solution to the Riemann problem are as follows:

- Regions I_0, II_0, and IV are identical to the Cases 13 - 15 except that the order of the shock/rarefaction and contact discontinuity is reversed in I_0 and II_0.
- Region V: Just like in Cases 4 – 6, this occurs when the path from the left state to the right state passes through a vacuum (i.e., when $\rho = 0$), and the transition often involves a sequence of waves. The only difference from Cases 4 - 6 is that, instead of following an R_a, the left state in these cases follows an S_a.

Below are the state spaces for Cases 16 - 18:

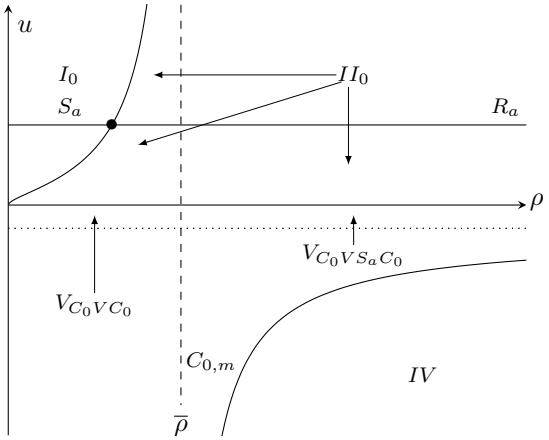

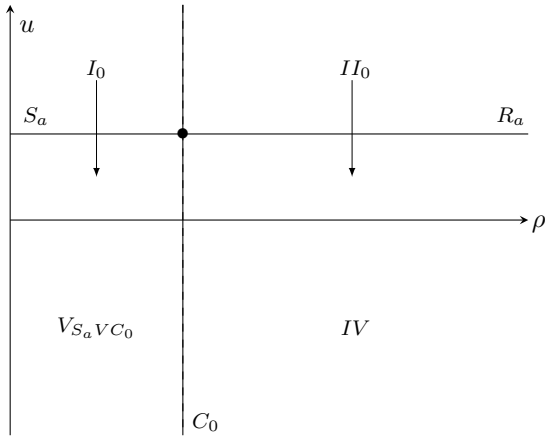

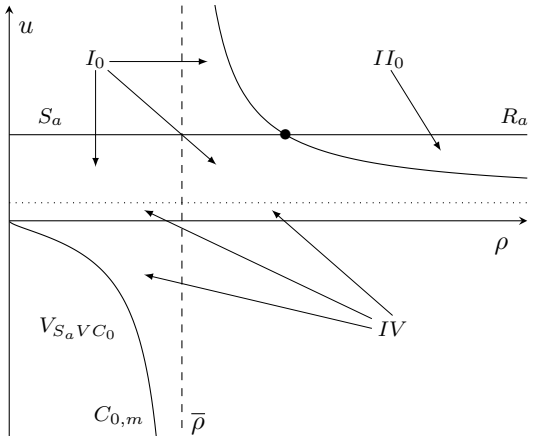

Figure 5:
Case 16: $\lambda_a > \lambda_0$ and $0 > \lambda_0$
Case 17: $\lambda_a > \lambda_0 = 0$
Case 18: $\lambda_a > \lambda_0 > 0$

4.3.3 $a = -1$

We again distinguish three cases:

- Case 7: $u_L < 0$ and $\rho_L < \overline{\rho}$,
- Case 8: $u_L < 0$ and $\rho_L = \overline{\rho}$, and
- Case 9: $u_L < 0$ and $\rho_L > \overline{\rho}$.

We now discuss the various regions for which different solutions exist and detail the path that is taken to reach the right state. For Cases 7 - 9, we have the following regions:

- Region III_a: The left state is connected to the right by an a-contact discontinuity followed by a 0-contact discontinuity.
- Region IV: The overcompressive region is similar to other negative values of a.
- Region VI: The left state will take an a-contact discontinuity to first reach $\overline{\rho}$ from Case 7 or Case 9, going into Case 8. It will then travel along $\overline{\rho}$ via a 0-contact discontinuity, followed by an a-contact discontinuity to the right state.

Below are the state spaces for Cases 7 - 9:

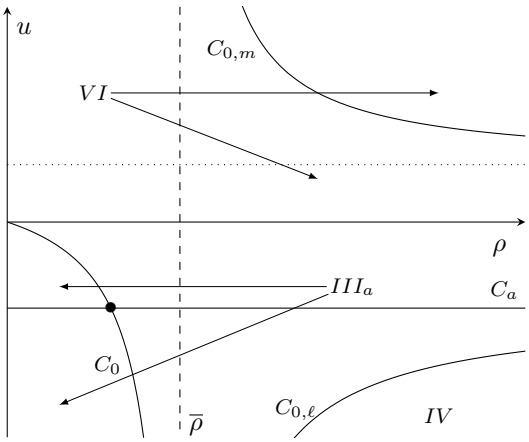

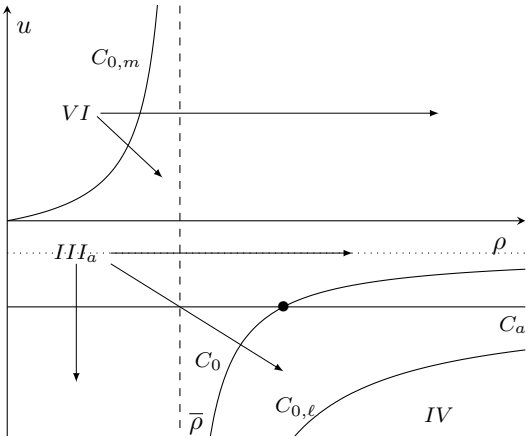

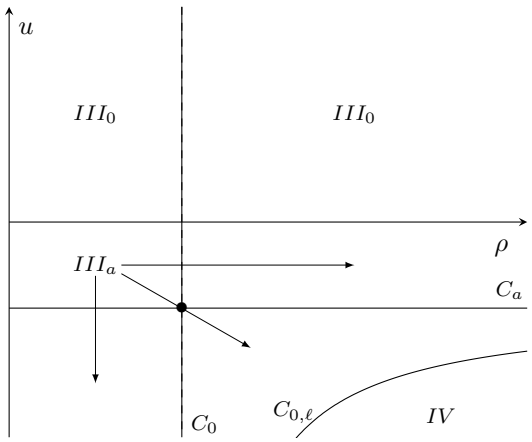

Figure 6:
Case 7 (above left): $\lambda_a < 0 < \lambda_0$
Case 8 (abover right): $\lambda_a < \lambda_0 = 0$
Case 9 (left) : $\lambda_a < \lambda_0 < 0$

We then turn to the following three cases:

- Case 10: $u_L > 0$ and $\rho_L < \overline{\rho}$,
- Case 11: $u_L > 0$ and $\rho_L = \overline{\rho}$, and
- Case 12: $u_L > 0$ and $\rho_L > \overline{\rho}$.

These are analogous to Cases 7, 8, and 9 except that $u_L > 0$, and also to Case 4, 5, 6, and Cases 16, 17, 18. The regions for the solution to the Riemann problem are as follows:

- Region III_0: The order of the contact discontinuities has now switched to C_0 followed by C_a.
- Region IV: The same behavior as the standard overcompressive regions, as in Cases 16 - 18.
- Region V: Just like in Cases 4 - 6 and Cases 16 - 18 except the a-shocks or a-rarefactions are now a-contact discontinuities.

Below are the state spaces for Cases 10 - 12:

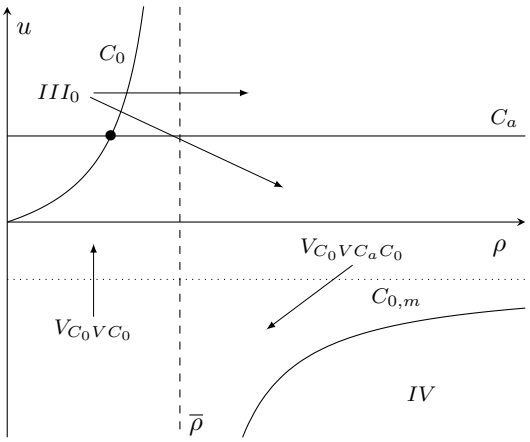

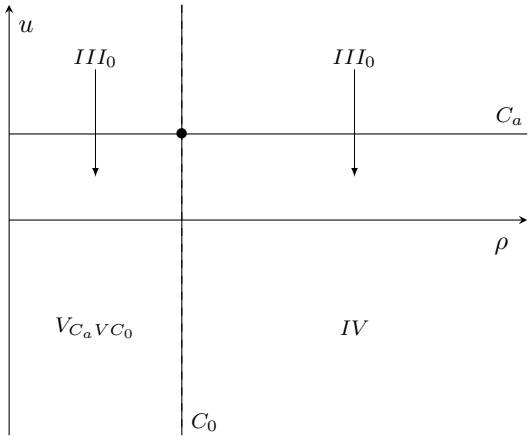

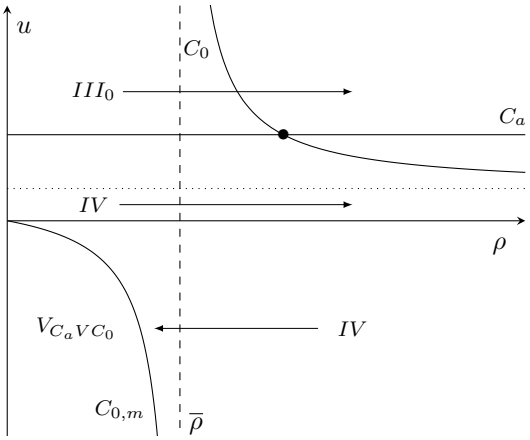

Figure 7:
Case 10 (above left): $\lambda_a > 0 > \lambda_0$
Case 11 (above right): $\lambda_a > \lambda_0 = 0$
Case 12 (left): $\lambda_a > \lambda_0 > 0$

4.3.4 $a > 0$

The last six cases are when $a > 0$.

- Case 19: $u_L < 0$ and $\rho_L < \overline{\rho}$,
- Case 20: $u_L < 0$ and $\rho_L = \overline{\rho}$, and
- Case 21: $u_L < 0$ and $\rho_L > \overline{\rho}$.

The various regions for the solution to the Riemann problem are

- Region I_0: The left state is connected to the right by a 0-contact discontinuity followed by an a-shock.
- Region II_0: The left state is connected to the right by a 0-contact discontinuity followed by an a-rarefaction.
- Region IV: The left state is connected to the right by an overcompressive delta-shock.
- Region V: The vacuum states can occur in multiple ways, first either following C_0 or S_a, and then staying on the line $\rho = 0$ for some nonzero time. When the solution can, it uses a 0-contact discontinuity, and otherwise an a-shock or a-rarefaction.

The following are the state spaces for Cases 19 - 21:

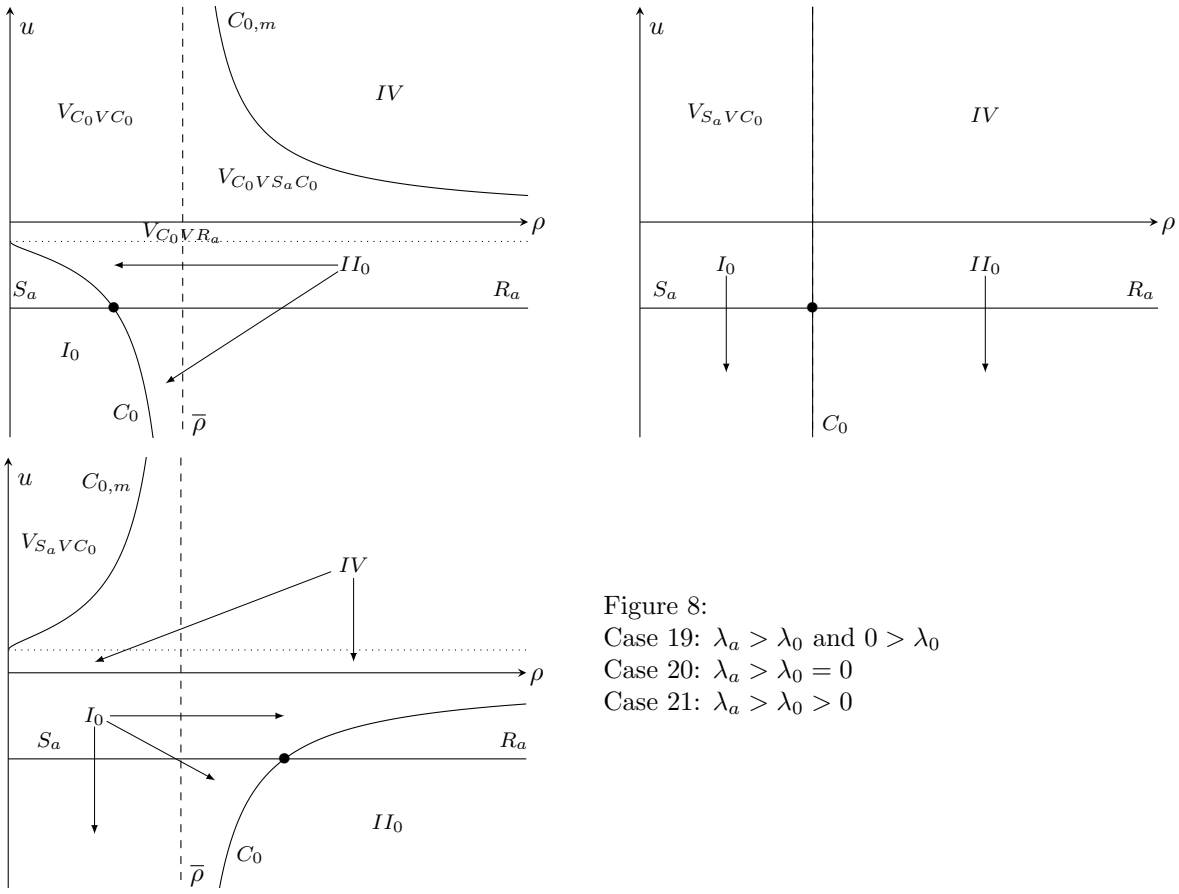

Figure 8:
Case 19: $\lambda_a > \lambda_0$ and $0 > \lambda_0$
Case 20: $\lambda_a > \lambda_0 = 0$
Case 21: $\lambda_a > \lambda_0 > 0$

Cases 22 through 24 are similar to the preceding three except that $u_L > 0$:

- Case 22: $u_L > 0$ and $\rho_L < \overline{\rho}$,
- Case 23: $u_L > 0$ and $\rho_L = \overline{\rho}$, and
- Case 24: $u_L > 0$ and $\rho_L > \overline{\rho}$.

The regions which exhibit a solution to the Riemann problem are as follows:

- Region I_a: The right state is reached by an a-shock followed by a 0-contact discontinuity;
- Region II_a: The right state is reached by an a-rarefaction followed by a 0-contact discontinuity;
- Region V: The left follows an a-rarefaction to reach a vacuum state, then a 0-contact discontinuity from the vacuum state to reach the right state.
- Region VI: The right state is reached by an a-shock from Case 22 and an a-rarefaction from Case 24, both into Case 23. It then follows a 0-contact discontinuity into Case 20.

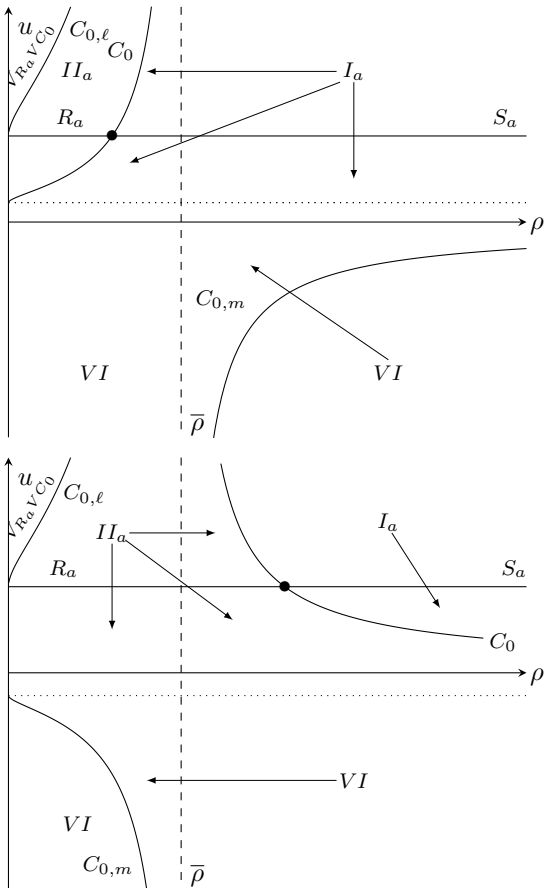

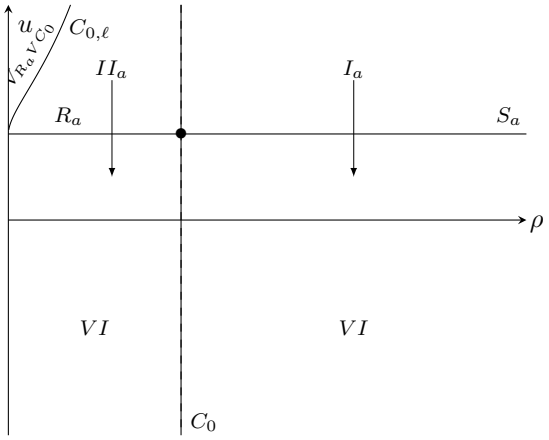

Figure 9:
Case 22: $\lambda_a < \lambda_0$ and $0 < \lambda_0$
Case 23: $\lambda_a < \lambda_0 = 0$
Case 24: $\lambda_a < \lambda_0 < 0$

5 Geometric Singular Perturbation Theory

In this section, we use geometric singular perturbation theory (GSPT), a central tool in the study of singularly perturbed systems, to establish the existence of self-similar viscous profiles for sufficiently small $\varepsilon > 0$, thus confirming the formation of overcompressive delta-shocks we have described in the previous sections. In our case, the solution consists of two distinct parts: an outer region, comprising the constant states (ρ_L, u_L) and (ρ_R, u_R), and an inner region that captures the transition layer on a rescaled fast time scale.

Normal hyperbolicity ensures that directions transverse to an invariant manifold dominate the dynamics and allows us to apply Fenichel's theory [7]. However, in the vicinity of specific critical points, this condition fails, complicating the analysis. Following Schecter's work [28], we introduced a blow-up transformation that regularizes the dynamics near the degenerate set, revealing hidden hyperbolic behavior. Our analysis begins by studying the system in the singular limit $\varepsilon = 0$, then uses the Exchange Lemma to guarantee the persistence of connecting orbits in the perturbed system when $\varepsilon > 0$ is small. By verifying the required transversality and non-degeneracy conditions, we show that the singular configuration, a concatenation of outer and inner layers, extends to a smooth orbit in the full system. This construction provides a rigorous justification for the appearance of overcompressive delta-shocks as singular limits of smooth viscous profiles.

Following [16, 28], we employ the Dafermos regularization, which preserves self-similar solutions to the traveling wave of the system. Specifically, we analyze the resulting equations in self-similar coordinates to study the existence and structure of viscous profiles. The regularized equations take the form

$$\begin{cases} \rho_t + \left[\rho u - \rho u \left(\frac{\rho}{\overline{\rho}}\right)^a\right]_x = \varepsilon t \rho_{xx}, & (5.1) \\ (\rho u)_t + \left[\rho u^2 - \rho u^2 \left(\frac{\rho}{\overline{\rho}}\right)^a\right]_x = \varepsilon t (\rho u)_{xx}. & (5.2) \end{cases}$$

The second-order terms introduced above are primarily analytical in nature. They are chosen so that the

regularized system remains compatible with the self-similar variable $\xi = x/t$, allowing the construction of profiles within the same similarity framework. These perturbations should therefore be viewed as a technical regularization rather than as additional physical modeling effects. In particular, the numerical experiments discussed in Culver et al. [5] are performed for the original system, and do not rely on the specific form of these higher-order corrections.

Remark 2. *The regularized formulation also provides a natural selection mechanism for the singular limit $\varepsilon \to 0$. The analysis does not assert uniqueness; rather, the regularization identifies a particular admissible δ-shock profile consistent with the self-similar structure of the problem. This construction should be interpreted as selecting a canonical solution within the present analytical framework rather than establishing a general uniqueness principle.*

Let $\xi = \frac{x}{t}$. Then, for any self-similar function $U(x,t) = U(\xi)$, we have $U_x = U_\xi \frac{\mathrm{d}\xi}{\mathrm{d}x} = \frac{1}{t} U_\xi$, $U_{xx} = \frac{\mathrm{d}}{\mathrm{d}x}\big(U_x\big)\frac{\mathrm{d}\xi}{\mathrm{d}x} = \frac{1}{t^2} U_{\xi\xi}$, and $U_t = U_\xi \frac{\mathrm{d}\xi}{\mathrm{d}t} = -\frac{x}{t^2} U_\xi$. Substituting these into the above regularized system and multiplying by t, we have

$$\begin{cases} -\xi\rho_\xi + \left[\rho u - \rho u \left(\frac{\rho}{\bar{\rho}}\right)^a\right]_\xi = \varepsilon\rho_{\xi\xi}, \\ -\xi(\rho u)_\xi + \left[\rho u^2 - \rho u^2 \left(\frac{\rho}{\bar{\rho}}\right)^a\right]_\xi = \varepsilon(\rho u)_{\xi\xi}. \end{cases} \tag{5.3}$$

The initial conditions from the Riemann problem translate, in the self-similar framework, to the following far-field conditions:

$$\begin{cases} (\rho, u)(-\infty) = (\rho_L, u_L), \\ (\rho, u)(+\infty) = (\rho_R, u_R). \end{cases} \tag{5.4}$$

From this point on, we proceed to work in vector notation and use $m = \rho u$. Let $U = (\rho \ \ m)^T$ and note that we now have

$$F(U) = \begin{pmatrix} F_1(U) \\ F_2(U) \end{pmatrix} = \begin{pmatrix} m - m\left(\frac{\rho}{\bar{\rho}}\right)^a \\ \frac{m^2}{\rho} - \frac{m^2}{\rho}\left(\frac{\rho}{\bar{\rho}}\right)^a \end{pmatrix}.$$

For convenience, we introduce $V = \varepsilon \begin{pmatrix} \frac{\mathrm{d}\rho}{\mathrm{d}\xi} & \frac{\mathrm{d}m}{\mathrm{d}\xi} \end{pmatrix}^T$ and the slow time $\vartheta = \xi - s_{\text{singular}}$, treating ξ as an additional state variable. Here s_{singular} denotes the shock speed introduced in (3.19) (i.e. $s_\pm$), and the shift $\vartheta = \xi - s_{\text{singular}}$ corresponds to moving into a frame centered at the singular wave. This increases the dimension but yields an autonomous system. Thus, we obtain, letting $'$ represent differentiation with respect to ϑ,

$$\begin{cases} \varepsilon U' = V, \\ \varepsilon V' = \big(DF(U) - \xi I\big)V, \\ \xi' = 1, \end{cases} \tag{5.5}$$

where DF is the Fréchet derivative of F with respect to the variables ρ and m.

As this is singular when $\varepsilon \to 0$ (higher-order derivatives vanish and the system drops to lower order), we introduce τ, the fast time such that $\vartheta = \varepsilon\tau$, and let $\dot{}$ represent differentiation with respect to τ. Then we have

$$\begin{cases} \dot{U} = V, \\ \dot{V} = \big(DF - \xi I\big)V, \\ \dot{\xi} = \varepsilon, \end{cases} \tag{5.6}$$

subject to the boundary conditions

$$\begin{cases} (U, V, \xi)(-\infty) = (U_L, 0, -\infty), \\ (U, V, \xi)(+\infty) = (U_R, 0, +\infty). \end{cases} \tag{5.7}$$

At $\varepsilon = 0$, this becomes

$$\begin{cases} \dot{U}_1 = V_1, \\ \dot{U}_2 = V_2, \\ \dot{V}_1 = \left(-\frac{am\rho^{a-1}}{\overline{\rho}^a} - \xi\right) V_1 + \left(1 - \left(\frac{\rho}{\overline{\rho}}\right)^a\right) V_2, \\ \dot{V}_2 = \left(-\frac{m^2}{\rho^2}\left(1 - \left(\frac{\rho}{\overline{\rho}}\right)^a\right) - \frac{am^2}{\rho}\frac{\rho^{a-1}}{\overline{\rho}^a}\right) V_1 + \left(\frac{2m}{\rho}\left(1 - \left(\frac{\rho}{\overline{\rho}}\right)^a\right) - \xi\right) V_2, \\ \dot{\xi} = 0. \end{cases} \tag{5.8}$$

Thus, the 3-dimensional space $S = \{(U, V, \xi) : V = 0\}$ consists of equilibria when $\varepsilon = 0$ and is an invariant subspace under (5.8) for every ε. In fact, for $\varepsilon > 0$, the dynamics in this space reduce to linear motion in the increasing ξ direction.

To analyze the structure near the equilibria, we linearize the full system around the fixed points $V = 0$, $\varepsilon = 0$. The Jacobian matrix at these points reveals eigenvalues $\lambda = 0$ with multiplicity three, corresponding to free directions in the components U and ξ. The remaining eigenvalues are real, nonzero when $a \neq 0$ and are given by $\lambda = \lambda_a - \xi$ and $\lambda = \lambda_0 - \xi$. Therefore, the linearization admits a full set of eigenvectors, ensuring the existence of a complete eigenbasis. Using the eigenvalues of (1.1) - (1.2), we identify two subsets of S: for $\delta > 0$, we define the 3-dimensional manifolds

$$S_0 = \left\{ \big(U, V, \xi\big) : \|U\| \leq \frac{1}{\delta}, V = 0, \xi \leq \min\{\lambda_a, \lambda_0\} - \delta \right\},$$
$$S_2 = \left\{ \big(U, V, \xi\big) : \|U\| \leq \frac{1}{\delta}, V = 0, \max\{\lambda_a, \lambda_0\} + \delta \leq \xi \right\}.$$

When $\lambda = -\xi + \lambda_a(U)$ and $\lambda = -\xi + \lambda_0(U)$, both eigenvalues are positive in S_0, and there is an unstable manifold of dimension 2 in S_0. In addition, both eigenvalues are negative in S_2, and there is a stable manifold of dimension 2 in S_2. Then $(U_L, 0, -\infty)$ is an α-limit of points in S_0, and $(U_R, 0, +\infty)$ is an ω-limit of points in S_2. Given a left state U_L, we define the 1-dimensional invariant set

$$S_0(U_L) = \left\{ \big(U, V, \xi\big) : U = U_L, V = 0, \xi < \min\{\lambda_a, \lambda_0\} \text{ at } U_L \right\}.$$

This line of equilibria admits a 3-dimensional unstable manifold $W^u_\varepsilon\big(S_0(U_L)\big)$, which is a perturbation of the unstable manifold

$$W^u_0\big(S_0(U_L)\big) = \left\{ \big(U, V, \xi\big) : U \in \Omega_\xi, V = V(U), \xi < \min\{\lambda_a, \lambda_0\} \text{ at } U_L \right\},$$

where Ω_ξ is an open subset of U-space depending on ξ and U_L. The function $V(U)$ is obtained by solving (5.6). Similarly, for a given right state U_R, we define the 1-dimensional set

$$S_2(U_R) = \left\{ \big(U, V, \xi\big) : U = U_R, V = 0, \max\{\lambda_a, \lambda_0\} < \xi \text{ at } U_R \right\},$$

which has a corresponding 3-dimensional stable manifold $W^s_\varepsilon\big(S_2(U_R)\big)$, the perturbation of

$$W^s_0\big(S_2(U_R)\big) = \left\{ \big(U, V, \xi\big) : U \in \Omega_\xi, V = V(U), \max\{\lambda_a, \lambda_0\} < \xi \text{ at } U_R \right\}.$$

Our objective is to demonstrate that the perturbed invariant manifolds $W^u_\epsilon\big(S_0(U_L)\big)$ and $W^s_\epsilon\big(S_2(U_R)\big)$ intersect transversely in the extended 5-dimensional phase space. (See Figure 10.) Any trajectory contained in this intersection corresponds to a heteroclinic orbit connecting the left state U_L as $\tau \to -\infty$ to the right state U_R as $\tau \to +\infty$, thus yielding a self-similar viscous profile.

To isolate the deviation from the Rankine–Hugoniot condition across the internal structure of the profile, we introduce the variable

$$W = -V + F(U) - \xi U, \tag{5.9}$$

so that $W = 0$ exactly when the classical Rankine-Hugoniot condition is satisfied for the shock speed $\xi = x'(t)$. Here $W = (w_1, w_2)^T$ denotes the vector of auxiliary variables, and w_1, w_2 refer to its individual

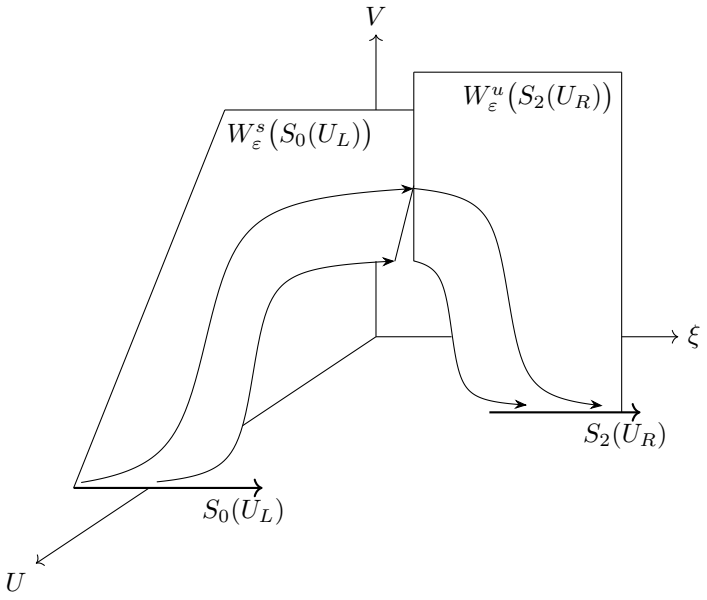

Figure 10: The objective of finding a heteroclinic orbit connecting the left state to the right state.

components. This change of variables isolates the jump structure and facilitates the analysis of the profile's internal structure. We also now treat ε as a state variable, and our system becomes

$$\begin{cases} \dot{U} = \big(F(U) - \xi U\big) - W, \\ \dot{W} = -\varepsilon U, \\ \dot{\xi} = \varepsilon, \\ \dot{\varepsilon} = 0. \end{cases} \tag{5.10}$$

We reformulate the problem in an extended 4-dimensional phase space with coordinates (U, W, ξ, ϵ). For each fixed $\varepsilon > 0$, the subspace $\varepsilon = \text{const.}$ is invariant. Within this setting, we define the following:

- Two normally hyperbolic invariant manifolds:

$$T_0 = \left\{ (U, W, \xi, \epsilon) : \|U\| \leq \frac{1}{\delta},\, W = F(U) - \xi U,\, \xi \leq \min\{\lambda_a, \lambda_0\} - \delta \right\},$$
$$T_2 = \left\{ (U, W, \xi, \epsilon) : \|U\| \leq \frac{1}{\delta},\, W = F(U) - \xi U,\, \max\{\lambda_a, \lambda_0\} + \delta \leq \xi \right\}.$$

- The reduced 1-dimensional invariant sets for the boundary states:

$$T_0^\epsilon(U_L) = \{(U, W, \xi, \epsilon) : U = U_L,\, W = F(U_L) - \xi U_L,\, \xi < \min\{\lambda_a, \lambda_0\} \text{ at } U_L\},$$
$$T_2^\epsilon(U_R) = \{(U, W, \xi, \epsilon) : U = U_R,\, W = F(U_R) - \xi U_R,\, \max\{\lambda_a, \lambda_0\} < \xi \text{ at } U_R\}.$$

- The associated 3-dimensional (un)stable manifolds:

$$W^u(T_0^\epsilon(U_L)) = \{(U, W, \xi, \epsilon) : U \in \Omega_\xi,\, W = W(U),\, \xi < \min\{\lambda_a, \lambda_0\} \text{ at } U_L\},$$
$$W^s(T_2^\epsilon(U_R)) = \{(U, W, \xi, \epsilon) : U \in \Omega_\xi,\, W = W(U),\, \max\{\lambda_a, \lambda_0\} < \xi \text{ at } U_R\},$$

  where Ω_ξ is an open subset of U-space depending on ξ, and $W(U)$ is the solution of (5.10).

Our goal is to show that the perturbed manifolds $W^u(T_0^\varepsilon(U_L))$ and $W^s(T_2^\varepsilon(U_R))$ intersect in the 5-dimensional extended phase space. Any such intersection corresponds to a viscous profile that connects U_L to U_R, representing a valid traveling wave solution for fixed $\varepsilon > 0$.

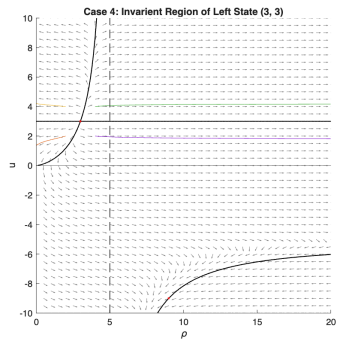

(a) Invariant region of left state

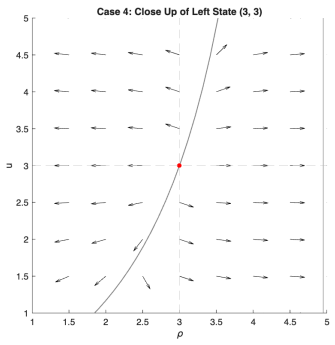

(b) Close up of left state invariant region

Figure 11: Case 4: Invariant Region of Left State. Left State: $(3, 3)$. Parameters: $\bar{\rho} = 5$, $a = -1.5$.

We now want to convert our system back to the variables ρ and $u = \frac{m}{\rho}$. We have $\dot{u} = \frac{\dot{m}}{\rho} - \frac{m}{\rho^2}\dot{\rho}$ and

$$\dot{U} = \begin{pmatrix} \dot{\rho} \\ \dot{m} \end{pmatrix} = \begin{pmatrix} m\left(1 - \left(\frac{\rho}{\bar{\rho}}\right)^a\right) - \xi\rho - w_1 \\ \frac{m^2}{\rho}\left(1 - \left(\frac{\rho}{\bar{\rho}}\right)^a\right) - \xi m - w_2 \end{pmatrix}.$$

Thus,

$$\begin{aligned} \dot{u} =& \frac{1}{\rho}\left\{\frac{m^2}{\rho}\left(1 - \left(\frac{\rho}{\bar{\rho}}\right)^a\right) - \xi m - w_2\right\} \\ & - \frac{m^2}{\rho}\left\{m\left(1 - \left(\frac{\rho}{\bar{\rho}}\right)^a\right) - \xi\rho - w_1\right\} \\ =& u^2\left(1 - \left(\frac{\rho}{\bar{\rho}}\right)^a\right) - \xi u - \frac{w_2}{\rho} - u^2\left(1 - \left(\frac{\rho}{\bar{\rho}}\right)^a\right) + u\xi + \frac{u}{\rho}w_1 \\ =& \frac{uw_1 - w_2}{\rho}. \end{aligned}$$

Our system then becomes

$$\begin{cases} \dot{\rho} = u\rho\left(1 - \left(\frac{\rho}{\bar{\rho}}\right)^a\right) - \xi\rho - w_1, \\ \dot{u} = \frac{uw_1 - w_2}{\rho}, \\ \dot{w_1} = -\varepsilon\rho, \\ \dot{w_2} = -\varepsilon\rho u, \\ \dot{\xi} = \varepsilon, \\ \dot{\varepsilon} = 0. \end{cases} \tag{5.11}$$

We also consider the reduced system from (5.10)

$$\dot{U} = F(U) - sU - W_L$$

When $\varepsilon = 0$, ξ is equal to the speed of the delta-shock $s = x'(t)$, $W_L = F(U_L) - sU_L$, and the equilibrium point U_L acts as a source.

Proposition 1. *The planar system $\dot{U} = F(U) - sU - W_L$ contains a negatively invariant region to the right of U_L, bounded by the contact discontinuity curve of the 0-family that passes through the left state and the straight line $u = u_L$ (see Figure 11).*

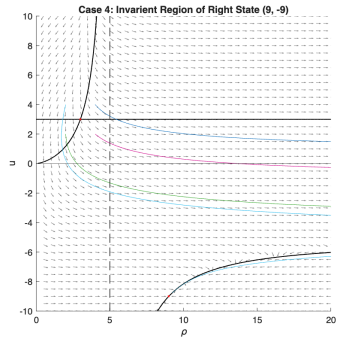

(a) Invariant region of left state

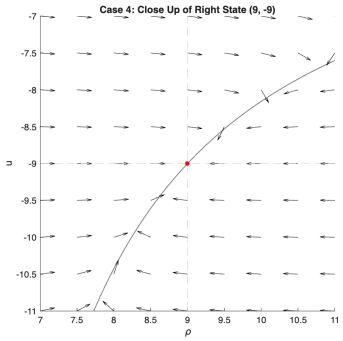

(b) Close up of right state invariant region

Figure 12: Case 4: Invariant Region of Right State. Right State: $(9, -9)$. Parameters: $\bar{\rho} = 5$, $a = -1.5$.

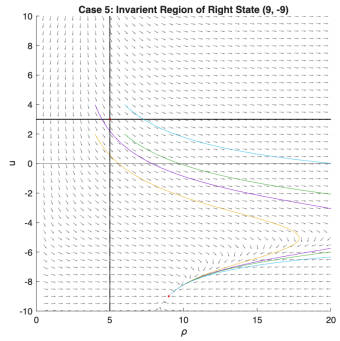

(a) Invariant region of right state

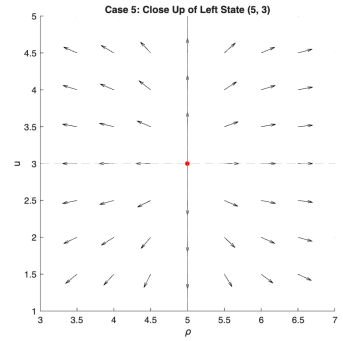

(b) Close up of left state invariant region

Figure 13: Case 5: Invariant Region of Right and Left States, where $\rho_L = \bar{\rho}$. Right State: $(9, -9)$. Left State: $(5, 3)$. Parameters: $\bar{\rho} = 5$, $a = -1.5$.

Proof. A direct computation of $\dot{U}$ along the curve and the horizontal line, using an argument analogous to Lemma 3.2 in [27], confirms that the vector field either points outward or is tangent to the boundary, following the curve or line precisely. Hence, the region is negatively invariant under the flow. □

Similarly, if we consider

$$\dot{U} = F(U) - sU - W_R$$

with $\varepsilon = 0$, $\xi = s$, and $W_R = F(U_R) - sU_R$, then the equilibrium U_R acts as a sink.

Proposition 2. *The planar system $\dot{U} = F(U) - sU - W_R$ contains a positively invariant region to the right of U_R, bounded by the contact discontinuity curve of the 0-family that passes through the right state and the straight line $u = u_R$ (see Figure 12).*

Proof. A calculation of $\dot{U}$ along the curve and line, again similar to Lemma 3.2 in [27], verifies the result. □

In particular, the first proposition implies that all the trajectories contained within the curvilinear wedge have U_L as their α-limit. Similarly, in the corresponding region near U_R, the trajectories have U_R as their ω-limit.

Note that these propositions still hold even when $\rho_L = \bar{\rho}$ or $\rho_R = \bar{\rho}$, as shown by Figures 13 and 14.

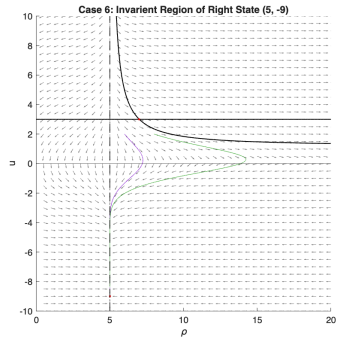

(a) Invariant region of right state

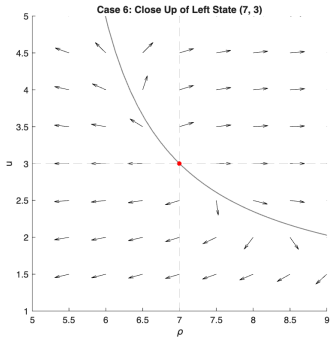

(b) Close up of left state invariant region

Figure 14: Case 6: Invariant Region of Right and Left States, where $\rho_R = \bar{\rho}$. Right State: $(5, -3)$. Left State: $(7, 3)$. Parameters: $\bar{\rho} = 5$, $a = -1.5$.

5.1 Delta-Shocks for $a < 0$: The Blow-up Procedure

Using the delta-shock predicted by Section 3.2.1, we now consider $\rho = \frac{\rho_0}{\varepsilon}$ (note that $\rho_0(\pm\infty) = 0$). Since ε is a constant with respect to τ, our system then becomes

$$\begin{cases} \dot{\rho_0} = u\rho_0 \left(1 - \left(\frac{\rho_0}{\varepsilon\bar{\rho}}\right)^a\right) - \xi\rho_0 - \varepsilon w_1, \\ \dot{u} = \frac{(uw_1 - w_2)\varepsilon}{\rho_0}, \\ \dot{w_1} = -\rho_0, \\ \dot{w_2} = -u\rho_0, \\ \dot{\xi} = \varepsilon, \\ \dot{\varepsilon} = 0. \end{cases} \tag{5.12}$$

When $\varepsilon = 0$, the system has a fixed point at $\rho_0 = 0$ (also note that $\dot{\rho_0} = (u - \xi)\rho_0$ and $\dot{u} = 0$). To analyze the dynamics near it, we first *desingularize*, which involves a rescaling of time. Specifically, we multiply the right-hand side of the system by a factor of ρ_0, effectively changing the time variable. This is not merely an algebraic manipulation: it corresponds to a change of time scale that slows down the flow near the singularity and reveals a hidden structure in the dynamics.

At the point $(\rho_0, u, \epsilon) = (0, \xi, 0)$, the fast system loses normal hyperbolicity. When we linearize the desingularized system at this equilibrium, we find that some eigenvalues of the Jacobian matrix vanish in directions transverse to the critical manifold. As a result, the classical theory of Fenichel does not apply. To analyze the dynamics near this degenerate point, we perform a blow-up transformation that replaces the singularity with a sphere. This transformation resolves the non-hyperbolic structure and reveals directions in different charts, allowing the use of tools such as the Exchange Lemma to rigorously track trajectories through this critical region. Thus, we introduce the *blow-up transformation* by setting

$$\rho_0 = r\,\overline{\rho}_0, \quad u - \xi = r\,\overline{u}_0, \quad \varepsilon = r\,\overline{\varepsilon}, \quad \text{with} \quad \overline{\rho}_0^2 + \overline{u}_0^2 + \overline{\varepsilon}^2 = 1.$$

At this stage, we note that

$$\begin{aligned}
\frac{\mathrm{d}\rho_0}{\mathrm{d}\tau} &= \frac{\mathrm{d}r}{\mathrm{d}\tau}\overline{\rho}_0 + r\frac{\mathrm{d}\overline{\rho}_0}{\mathrm{d}\tau} \\
&= r\overline{\rho}_0(r\overline{u}_0+\xi) - r\overline{\rho}_0(r\overline{u}_0+\xi)\left(\frac{r\overline{\rho}_0}{r\overline{\varepsilon}\,\overline{\rho}}\right)^a - \xi r\overline{\rho}_0 - r\overline{\varepsilon}w_1, \\
\Longrightarrow\ \frac{\mathrm{d}\overline{\rho}_0}{\mathrm{d}\tau} &= -\frac{\overline{\rho}_0}{r}\frac{\mathrm{d}r}{\mathrm{d}\tau} + \overline{\rho}_0(r\overline{u}_0+\xi) - \overline{\rho}_0(r\overline{u}_0+\xi)\left(\frac{\overline{\rho}_0}{\overline{\varepsilon}\,\overline{\rho}}\right)^a - \xi\overline{\rho}_0 - \overline{\varepsilon}w_1; \\
\frac{\mathrm{d}(u-\xi)}{\mathrm{d}\tau} &= \frac{\mathrm{d}r}{\mathrm{d}\tau}\overline{u}_0 + r\frac{\mathrm{d}\overline{u}_0}{\mathrm{d}\tau} = \frac{\big((r\overline{u}_0+\xi)w_1 - w_2\big)r\overline{\varepsilon}}{r\overline{\rho}_0} - r\overline{\varepsilon}, \\
\Longrightarrow\ \frac{\mathrm{d}\overline{u}_0}{\mathrm{d}\tau} &= -\frac{\overline{u}_0}{r}\frac{\mathrm{d}r}{\mathrm{d}\tau} + \frac{\big((r\overline{u}_0+\xi)w_1 - w_2\big)\overline{\varepsilon}}{r\overline{\rho}_0} - \overline{\varepsilon}; \\
0 = \frac{\mathrm{d}\varepsilon}{\mathrm{d}\tau} &= \frac{\mathrm{d}r}{\mathrm{d}\tau}\overline{\varepsilon} + r\frac{\mathrm{d}\overline{\varepsilon}}{\mathrm{d}\tau} \ \Longrightarrow\ \frac{\mathrm{d}\overline{\varepsilon}}{\mathrm{d}\tau} = -\frac{\varepsilon}{r}\frac{\mathrm{d}r}{\mathrm{d}\tau}.
\end{aligned}$$

Combining these with the relation $\overline{\rho}_0\dot{\overline{\rho}}_0 + \overline{u}_0\dot{\overline{u}}_0 + \overline{\varepsilon}\,\dot{\overline{\varepsilon}} = 0$, we obtain

$$\frac{\mathrm{d}r}{\mathrm{d}\tau} = \frac{\big((r\overline{u}_0+\xi)w_1 - w_2\big)\overline{\varepsilon}\,\overline{u}_0}{\overline{\rho}_0} - r\overline{\varepsilon}\,\overline{u}_0 + r\overline{\rho}_0^2(r\overline{u}_0+\xi)\left(1-\left(\frac{\overline{\rho}_0}{\overline{\varepsilon}\,\overline{\rho}}\right)^a\right) - \xi r\overline{\rho}_0^2 - r\overline{\varepsilon}\,\overline{\rho}_0 w_1.$$

Upon substituting the blow-up transformation into the previously derived system, we obtain a reformulated system where r appears explicitly as an additional variable

$$\begin{cases}
\frac{\mathrm{d}r}{\mathrm{d}\tau} = \frac{\big((r\overline{u}_0+\xi)w_1-w_2\big)\overline{\varepsilon}\,\overline{u}_0}{\overline{\rho}_0} - r\overline{\varepsilon}\,\overline{u}_0 + r\overline{\rho}_0^2(r\overline{u}_0+\xi)\left(1-\left(\frac{\overline{\rho}_0}{\overline{\varepsilon}\,\overline{\rho}}\right)^a\right) - \xi r\overline{\rho}_0^2 - r\overline{\varepsilon}\,\overline{\rho}_0 w_1, \\
\frac{\mathrm{d}\overline{\rho}_0}{\mathrm{d}\tau} = \overline{\rho}_0(r\overline{u}_0+\xi)\left(1-\left(\frac{\overline{\rho}_0}{\overline{\varepsilon}\,\overline{\rho}}\right)^a\right) - \xi\overline{\rho}_0 - \overline{\varepsilon}w_1 - \frac{\big((r\overline{u}_0+\xi)w_1-w_2\big)\overline{\varepsilon}\,\overline{u}_0}{r} + \overline{\varepsilon}\,\overline{\rho}_0\,\overline{u}_0 \\
\qquad -\overline{\rho}_0^3(r\overline{u}_0+\xi)\left(1-\left(\frac{\overline{\rho}_0}{\overline{\varepsilon}\,\overline{\rho}}\right)^a\right) + \xi\,\overline{\rho}_0^3 + \overline{\varepsilon}\,\overline{\rho}_0^2 w_1, \\
\frac{\mathrm{d}\overline{u}_0}{\mathrm{d}\tau} = \frac{\big((r\overline{u}_0+\xi)w_1-w_2\big)\overline{\varepsilon}}{r\overline{\rho}_0} - \overline{\varepsilon} - \frac{\big((r\overline{u}_0+\xi)w_1-w_2\big)\overline{\varepsilon}\,\overline{u}_0^2}{r\overline{\rho}_0} + \overline{\varepsilon}\,\overline{u}_0^2 + \xi\,\overline{\rho}_0^2\,\overline{u}_0 \\
\qquad -\overline{\rho}_0^2\,\overline{u}_0(r\overline{u}_0+\xi)\left(1-\left(\frac{\overline{\rho}_0}{\overline{\varepsilon}\,\overline{\rho}}\right)^a\right) - \overline{\varepsilon}\,\overline{\rho}_0\overline{u}_0 w_1, \\
\frac{\mathrm{d}\overline{\varepsilon}}{\mathrm{d}\tau} = -\frac{\big((r\overline{u}_0+\xi)w_1-w_2\big)\overline{\varepsilon}^2\overline{u}_0}{r\overline{\rho}_0} + \overline{\varepsilon}^2\overline{u}_0 - \overline{\varepsilon}\,\overline{\rho}_0^2(r\overline{u}_0+\xi)\left(1-\left(\frac{\overline{\rho}_0}{\overline{\varepsilon}\,\overline{\rho}}\right)^a\right) + \xi\,\overline{\varepsilon}\,\overline{\rho}_0^2 + \overline{\varepsilon}^2\overline{\rho}_0 w_1, \\
\frac{\mathrm{d}w_1}{\mathrm{d}\tau} = -r\overline{\rho}_0, \\
\frac{\mathrm{d}w_2}{\mathrm{d}\tau} = -r\overline{\rho}_0(r\overline{u}_0+\xi), \\
\frac{\mathrm{d}\xi}{\mathrm{d}\tau} = r\overline{\varepsilon}.
\end{cases} \tag{5.13}$$

We proceed with a second desingularization (multiplying by r and $\overline{\rho}_0 \geq 0$ and dividing by $\overline{\varepsilon} \geq 0$) and then

linearize the resulting system and evaluate it at $r = 0$, which yields

$$\begin{cases} \frac{\mathrm{d}r}{\mathrm{d}\tau} = 0 = \frac{\mathrm{d}w_1}{\mathrm{d}\tau} = \frac{\mathrm{d}w_2}{\mathrm{d}\tau} = \frac{\mathrm{d}\xi}{\mathrm{d}\tau}, \\ \frac{\mathrm{d}\overline{\rho}_0}{\mathrm{d}\tau} = -\overline{u}_0\,\overline{\rho}_0\,(\xi w_1 - w_2)\,, \\ \frac{\mathrm{d}\overline{u}_0}{\mathrm{d}\tau} = (\xi w_1 - w_2)\left(1 - \overline{u}_0^2\right), \\ \frac{\mathrm{d}\overline{\varepsilon}}{\mathrm{d}\tau} = -\overline{\varepsilon}\,\overline{u}_0\,(\xi w_1 - w_2)\,. \end{cases} \tag{5.14}$$

Note that before setting $r = 0$ we have the equation for the radial variable $\frac{\mathrm{d}r}{\mathrm{d}\tau} = \big(\xi w_1 - w_2\big)\overline{u}_0 r + O(r^2)$, which governs the behavior of trajectories near the sphere. Recall now that $\frac{\mathrm{d}w_1}{\mathrm{d}\tau} = -\rho_0$, so

$$w_1(\tau) = -\int_{-\infty}^{\tau} \rho_0(s)\mathrm{d}s + w_1(-\infty).$$

Likewise, since $\frac{\mathrm{d}w_2}{\mathrm{d}\tau} = -\rho_0 u$, we have

$$\begin{aligned} w_2(\tau) &= -\int_{-\infty}^{\tau} \rho_0 u \mathrm{d}s + w_2(-\infty) \\ &= w_2(-\infty) - \int_{-\infty}^{\tau} u\mathrm{d}\left(\int_{-\infty}^{s} \rho_0 \mathrm{d}\theta\right) \\ &= w_2(-\infty) - \left(u\int_{-\infty}^{s} \rho_0 \mathrm{d}\theta\right)\Big|_{-\infty}^{\tau} + \int_{-\infty}^{\tau}\left\{\frac{\mathrm{d}u(s)}{\mathrm{d}s}\int_{-\infty}^{s}\rho_0\mathrm{d}\theta\right\}\mathrm{d}s. \end{aligned}$$

Using that

$$\begin{aligned} w_2(-\infty) &= -V_{2,L} + F_2(U_L) - \xi U_{2,L} \\ &= -0 + \rho_L u_L^2\left(1 - \left(\frac{\rho_L}{\overline{\rho}}\right)^a\right) - \xi\rho_L u_L \\ &= u_L\left(\rho_L u_L\left(1 - \left(\frac{\rho_L}{\overline{\rho}}\right)^a\right) - \xi\rho_L\right) \\ &= u_L w_1(-\infty), \end{aligned}$$

we obtain

$$\xi w_1 - w_2 = (\xi - u_L)w_1(-\infty) - (\xi - u)\int_{\infty}^{\tau}\rho_0\mathrm{d}s - \int_{-\infty}^{\tau}\left\{\frac{\mathrm{d}u(s)}{\mathrm{d}s}\int_{-\infty}^{s}\rho_0\mathrm{d}\theta\right\}\mathrm{d}s.$$

When $r = 0$ (which corresponds to $\varepsilon = 0$) and $u = \xi$ (with ξ constant and equal to the speed of the delta-shock), the expression simplifies to

$$\xi w_1 - w_2 = (\xi - u_L)w_1(-\infty) = (\xi - u_L)\rho_L\left(u_L\left(1 - \left(\frac{\rho_L}{\overline{\rho}}\right)^a\right) - \xi\right),$$

which is negative in the inner layer. This holds because $\rho_L > 0$, $\xi < \lambda_0(U_L)$ (assumed in equation (3.19)), and $\xi < u_L$. As we discussed in Section 4, in each of the different cases, any region such that $u_R > u_L$ is accessible when $a < 0$ via classical waves. Thus, if a delta-shock appeared (which we know does), it must be the case that $u_R < \xi < u_L$. We then return to (5.13), desingularize once more by dividing by $-(\xi w_1 - w_2)$ (which corresponds to a rescaling of time), let $r = 0$, and observe that the points $\overline{u}_0 = \pm 1$ with $\overline{\rho}_0 = \overline{\varepsilon} = 0$ are fixed points. Linearizing the system about the fixed points $\overline{u}_0 = \pm 1$ and $\overline{\rho}_0 = \overline{\varepsilon} = 0$ yields eigenvalues $\lambda = \overline{u}_0, 2\overline{u}_0, \overline{u}_0,$ and $-\overline{u}_0$ in the $\overline{\rho}_0, \overline{u}_0, \overline{\varepsilon},$ and r directions, respectively. We again note that $\frac{\mathrm{d}r}{\mathrm{d}\tau} = -\overline{u}_0 r + O(r^2)$. This expression indicates that when $\overline{u}_0 = 1$, we have $\frac{dr}{d\tau} = -r + \mathcal{O}(r^2) < 0$ for small $r > 0$, so trajectories enter the blown up sphere transversely near the point $\overline{u}_0 = 1$; when $\overline{u}_0 = -1$, we have $\frac{dr}{d\tau} = r + \mathcal{O}(r^2) > 0$, so trajectories exit the sphere transversely near $\overline{u}_0 = -1$.

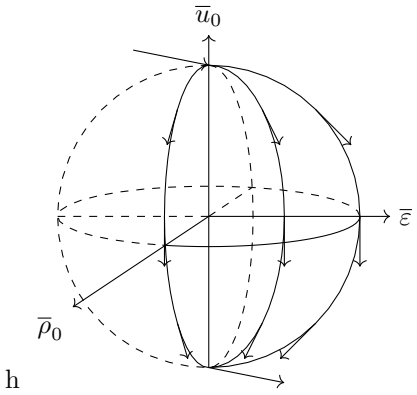

Figure 15: Illustration of the blow-up transformation and the inner solutions

The eigenvalues of the system on the blown-up sphere are nonzero, and the linearization yields a full set of linearly independent eigenvectors. Therefore, the fixed points are normally hyperbolic, and Fenichel's theory ensures the persistence of stable and unstable manifolds under perturbation.

We seek a heteroclinic orbit on the blown-up sphere connecting the fixed points $\overline{u}_0 = 1$ and $\overline{u}_0 = -1$. Since the flow on the sphere is regular after desingularization, such a connecting orbit corresponds to the inner solution of a viscous profile. The flow for $\overline{u}_0 \in (-1, 1)$ satisfies $\frac{\mathrm{d}\overline{u}_0}{\mathrm{d}\tau} = -(1 - \overline{u}_0^2) < 0$ and $\frac{\mathrm{d}\overline{\rho}_0}{\mathrm{d}\tau} = \overline{u}_0\overline{\rho}_0$, which implies that the system flows from $\overline{u}_0 = 1$ to $\overline{u}_0 = -1$ in the sphere. Therefore, there exists a heteroclinic orbit on the blown-up sphere connecting the north pole to the south pole. See Figure 15. This orbit corresponds to the inner layer of the delta-shock profile. The Exchange Lemma ensures that this connection persists for sufficiently small $\varepsilon > 0$. Specifically, since the entry and exit points are normally hyperbolic and the dimensions of the corresponding stable and unstable manifolds match (both of dimension 3), a transverse intersection of these manifolds implies the existence of a trajectory in the perturbed system connecting the left and right states.

A delta-shock solution is numerically represented in Figure 16 for Case 6, where $\rho_L > \overline{\rho}$, $u_L > 0$, and $a = -1.5$. As shown in the figure, the solution shows the density forming a progressively narrower, taller peak at the interface, indicating convergence toward a delta-shock solution as the left state connects to the right state. The solution to u decreases monotonically from u_L to u_R, however it slows to near rest when the delta-shock occurs.

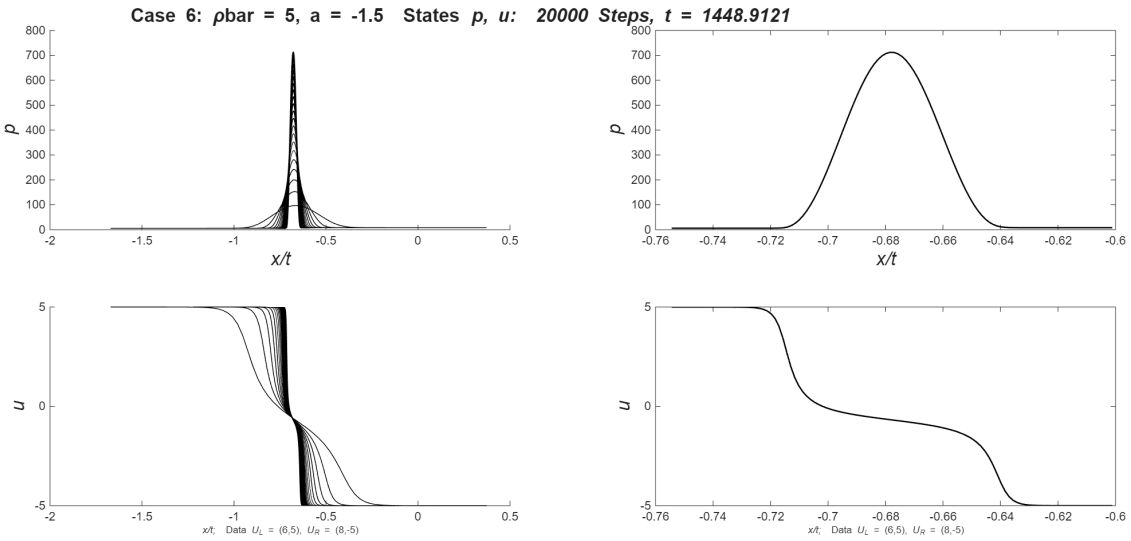

Figure 16: Right State: (6,5). Region IV. S_δ for $a < 0$

5.2 Delta-Shocks for $a > 0$: The Blow-up Procedure

Again, following the suggested values from the shadow wave analysis in Section 3.2.2, we consider $\rho = \frac{\rho_0}{\varepsilon}$ when $a > 0$. We substitute this into the system (5.11) and obtain

$$\begin{cases} \frac{\mathrm{d}\rho_0}{\mathrm{d}\tau} = \rho_0 u \left(1 - \left(\frac{\rho_0}{\varepsilon\overline{\rho}}\right)^a\right) - \xi\rho_0 - \varepsilon w_1, \\ \dot{u} = \frac{(uw_1 - w_2)}{\rho_0}\varepsilon, \\ \dot{w_1} = -\rho_0, \\ \dot{w_2} = -\rho_0 u, \\ \dot{\xi} = \varepsilon, \\ \dot{\varepsilon} = 0. \end{cases} \tag{5.15}$$

Note that if $u = \varepsilon^a u_0$, as discussed in Section 3.2.2, then $\frac{\mathrm{d}\rho_0}{\mathrm{d}\tau} = -\rho_0 u_0 \left(\frac{\rho_0}{\overline{\rho}}\right)^a - \xi\rho_0$ when $\varepsilon = 0$. Again we proceed with our blow-up procedure. Noting that the value of u at which the singularity occurred according to the shadow wave analysis was $u = 0$, let $\rho_0 = r^{k_1}\overline{\rho}_0, u = r^{k_2}\overline{u}_0, \varepsilon = r^{k_3}\overline{\varepsilon}$ subject to the constraint $\overline{u}_0^2 + \overline{\rho}_0^2 + \overline{\varepsilon}^2 = 1$, where $k_i \in \mathbb{R}_+$ are scaling exponents to be determined based on the balancing of leading-order terms in the blown-up equations.

Observe that

$$\begin{aligned} \frac{\mathrm{d}\rho_0}{\mathrm{d}\tau} &= k_1 r^{k_1-1}\frac{\mathrm{d}r}{\mathrm{d}\tau}\overline{\rho}_0 + r^{k_1}\frac{\mathrm{d}\overline{\rho}_0}{\mathrm{d}\tau} \\ &= r^{k_1}\overline{\rho}_0 r^{k_2}\overline{u}_0\left(1 - \left(\frac{r^{k_1}\,\overline{\rho}_0}{r^{k_3}\,\overline{\varepsilon}\,\overline{\rho}}\right)^a\right) - \xi r^{k_1}\,\overline{\rho}_0 - r^{k_3}\,\overline{\varepsilon}w_1, \\ \implies \frac{\mathrm{d}\overline{\rho}_0}{\mathrm{d}\tau} &= -\frac{k_1\overline{\rho}_0}{r}\frac{\mathrm{d}r}{\mathrm{d}\tau} + \overline{\rho}_0\overline{u}_0 r^{k_2}\left(1 - r^{(ak_1-ak_3)}\left(\frac{\overline{\rho}_0}{\overline{\varepsilon}\,\overline{\rho}}\right)^a\right) - \xi\overline{\rho}_0 - r^{k_3-k_1}\,\overline{\varepsilon}w_1; \\ \frac{\mathrm{d}u}{\mathrm{d}\tau} &= k_2 r^{k_2-1}\frac{\mathrm{d}r}{\mathrm{d}\tau}\overline{u}_0 + r^{k_2}\frac{\mathrm{d}\overline{u}_0}{\mathrm{d}\tau} = \frac{\left(r^{k_2}\overline{u}_0 w_1 - w_2\right)r^{k_3}\,\overline{\varepsilon}}{r^{k_1}\overline{\rho}_0}, \\ \implies \frac{\mathrm{d}\overline{u}_0}{\mathrm{d}\tau} &= -\frac{k_2\overline{u}_0}{r}\frac{\mathrm{d}r}{\mathrm{d}\tau} + \frac{\left(r^{k_2}\overline{u}_0 w_1 - w_2\right)}{\overline{\rho}_0}r^{(k_3-k_1-k_2)}\overline{\varepsilon}; \\ 0 = \frac{\mathrm{d}\varepsilon}{\mathrm{d}\tau} &= k_3 r^{(k_3-1)}\frac{\mathrm{d}r}{\mathrm{d}\tau}\overline{\varepsilon} + r^{k_3}\frac{\mathrm{d}\overline{\varepsilon}}{\mathrm{d}\tau} \implies \frac{\mathrm{d}\overline{\varepsilon}}{\mathrm{d}\tau} = -\frac{k_3\overline{\varepsilon}}{r}\frac{\mathrm{d}r}{\mathrm{d}\tau}. \end{aligned}$$

Let $\kappa = k_1\overline{\rho}_0^2 + k_2\overline{u}_0^2 + k_3\overline{\varepsilon}^2$. Using our relation $\overline{u}_0\dot{\overline{u}}_0 + \overline{\rho}_0\dot{\overline{\rho}}_0 + \overline{\varepsilon}\,\dot{\overline{\varepsilon}}_0 = 0$, we obtain

$$\begin{aligned} \kappa\frac{\mathrm{d}r}{\mathrm{d}\tau} = &\frac{\overline{u}_0\left(r^{k_2}\overline{u}_0 w_1 - w_2\right)\overline{\varepsilon}}{\overline{\rho}_0}r^{(k_3-k_1-k_2+1)} + \overline{\rho}_0^2\overline{u}_0 r^{(k_2+1)}\left(1 - r^{(ak_1-ak_3)}\left(\frac{\overline{\rho}_0}{\overline{\varepsilon}\,\overline{\rho}}\right)^a\right) \\ &- \xi r\overline{\rho}_0^2 - \overline{\rho}_0 r^{(k_3-k_1+1)}\,\overline{\varepsilon}w_1. \end{aligned}$$

The full system is

$$
\begin{cases}
\frac{\mathrm{d}r}{\mathrm{d}\tau} = \frac{1}{\kappa}\frac{\overline{u}_0\left(r^{k_2}\overline{u}_0w_1-w_2\right)\overline{\varepsilon}}{\overline{\rho}_0}r^{(k_3-k_1-k_2+1)} + \frac{1}{\kappa}\overline{\rho}_0^2\overline{u}_0r^{(k_2+1)}\left(1-r^{ak_1-ak_3}\left(\frac{\overline{\rho}_0}{\overline{\varepsilon}\,\overline{\rho}}\right)^a\right) \\
\qquad -\frac{1}{\kappa}\xi r\overline{\rho}_0^2 - \frac{1}{\kappa}\overline{\rho}_0r^{(k_3-k_1+1)}\,\overline{\varepsilon}w_1, \\
\frac{\mathrm{d}\overline{\rho}_0}{\mathrm{d}\tau} = -\frac{k_1}{\kappa}\overline{u}_0\left(r^{k_2}\overline{u}_0w_1-w_2\right)\overline{\varepsilon}r^{(k_3-k_1-k_2)} - \frac{k_1}{\kappa}\overline{\rho}_0^3\overline{u}_0r^{k_2}\left(1-r^{ak_1-ak_3}\left(\frac{\overline{\rho}_0}{\overline{\varepsilon}\,\overline{\rho}}\right)^a\right) \\
\qquad +\frac{k_1}{\kappa}\xi\overline{\rho}_0^3 + \frac{k_1}{\kappa}r^{(k_3-k_1)}\overline{\rho}_0^2\overline{\varepsilon}w_1 + \overline{\rho}_0\overline{u}_0r^{k_2}\left(1-r^{ak_1-ak_3}\left(\frac{\overline{\rho}_0}{\overline{\varepsilon}\,\overline{\rho}}\right)^a\right) - \xi\overline{\rho}_0 - r^{(k_3-k_1)}\,\overline{\varepsilon}w_1, \\
\frac{\mathrm{d}\overline{u}_0}{\mathrm{d}\tau} = -\frac{k_2}{\kappa}\frac{\overline{u}_0^2\left(r^{k_2}\overline{u}_0w_1-w_2\right)\overline{\varepsilon}}{\overline{\rho}_0}r^{(k_3-k_1-k_2)} - \frac{k_2}{\kappa}\overline{\rho}_0^2\overline{u}_0^2r^{k_2}\left(1-r^{ak_1-ak_3}\left(\frac{\overline{\rho}_0}{\overline{\varepsilon}\,\overline{\rho}}\right)^a\right) \\
\qquad +\frac{k_2}{\kappa}\xi\overline{\rho}_0^2\overline{u}_0 + \frac{k_2}{\kappa}\overline{\rho}_0\overline{u}_0r^{(k_3-k_1)}\,\overline{\varepsilon}w_1 + \frac{\left(r^{k_2}\overline{u}_0w_1-w_2\right)}{\overline{\rho}_0}r^{(k_3-k_1-k_2)}\overline{\varepsilon}, \\
\frac{\mathrm{d}\overline{\varepsilon}}{\mathrm{d}\tau} = -\frac{k_3}{\kappa}\frac{\overline{u}_0\left(r^{k_2}\overline{u}_0w_1-w_2\right)\overline{\varepsilon}^2}{\overline{\rho}_0}r^{(k_3-k_1-k_2)} - \frac{k_3}{\kappa}\overline{\rho}_0^2\overline{u}_0r^{k_2}\overline{\varepsilon}\left(1-r^{ak_1-ak_3}\left(\frac{\overline{\rho}_0}{\overline{\varepsilon}\,\overline{\rho}}\right)^a\right) \\
\qquad +\frac{k_3}{\kappa}\xi\,\overline{\varepsilon}\,\overline{\rho}_0^2 + \frac{k_3}{\kappa}\overline{\rho}_0r^{(k_3-k_1)}\overline{\varepsilon}^2w_1, \\
\frac{\mathrm{d}w_1}{\mathrm{d}\tau} = -r^{k_1}\overline{\rho}_0, \\
\frac{\mathrm{d}w_2}{\mathrm{d}\tau} = -r^{k_2+k_1}\overline{u}_0\overline{\rho}_0, \\
\frac{\mathrm{d}\xi}{\mathrm{d}\tau} = r^{k_3}\overline{\varepsilon}.
\end{cases}
\tag{5.16}
$$

Now, let $k_3 = k_2 = k_1 = 1 = \kappa$. Desingularize once again by multiplying by r and $\overline{\rho}_0$ and divide by $\overline{\varepsilon}$ (which corresponds to a rescaling of time). The first equation, for the radial variable, is now $\frac{\mathrm{d}r}{\mathrm{d}\tau} = -\overline{u}_0w_2r + O(r^2)$. Similar to the case $a<0$, since $\frac{\mathrm{d}w_2}{\mathrm{d}\tau} = -\rho_0u$, we once again have

$$
w_2(\tau) = u_Lw_1(-\infty) - \left(u\int_{-\infty}^{s}\rho_0\mathrm{d}\theta\right)\Big|_{-\infty}^{\tau} + \int_{-\infty}^{\tau}\left\{\frac{\mathrm{d}u(s)}{\mathrm{d}s}\int_{-\infty}^{s}\rho_0\mathrm{d}\theta\right\}\mathrm{d}s.
$$

When $r=0$ and $u=0$ (with ξ equal to the speed of the delta-shock, s_+), we get

$$
w_2(\tau) = u_L\rho_L\left(u_L\left(1-\left(\frac{\rho_L}{\overline{\rho}}\right)^a\right) - \xi\right),
$$

which is negative in the inner layer, because $\xi < \lambda_0(U_L)$ and $u_L<0$, the latter of which is observed in Section 4. We then desingularize by dividing with $-w_2$ and substitute $r=0$ to get

$$
\begin{cases}
\frac{\mathrm{d}\overline{\rho}_0}{\mathrm{d}\tau} = -\overline{\rho}_0\overline{u}_0, \\
\frac{\mathrm{d}\overline{u}_0}{\mathrm{d}\tau} = -\overline{u}_0^2+1, \\
\frac{\mathrm{d}\overline{\varepsilon}}{\mathrm{d}\tau} = -\overline{u}_0\overline{\varepsilon}, \\
\frac{\mathrm{d}w_1}{\mathrm{d}\tau} = 0 = \frac{\mathrm{d}w_2}{\mathrm{d}\tau} = \frac{\mathrm{d}\xi}{\mathrm{d}\tau}.
\end{cases}
\tag{5.17}
$$

We observe that the system has fixed points at $\overline{u}_0 = \pm 1$ with $\overline{\rho}_0 = \overline{\varepsilon} = 0$. These correspond to the entry and exit points of the blown-up sphere during the matching procedure of the inner and outer solutions. To study the behavior near these fixed points, we linearize the system around them. At $\overline{u}_0 = 1$, the eigenvalues are $-\overline{u}_0$, $-2\overline{u}_0$, and $-\overline{u}_0$ in the $\overline{\rho}_0$, $\overline{u}_0$, and $\overline{\varepsilon}$ directions, respectively. At $\overline{u}_0 = -1$, the eigenvalues become 1, 2, and 1. In analogy to the construction of Section 5.1, the point $\overline{u}_0 = -1$ serves as the entry point into the blown-up sphere along the unstable manifold, while the point $\overline{u}_0 = 1$ serves as the exit point along the stable manifold. The nonzero eigenvalues and the full set of eigenvectors ensure normal hyperbolicity, confirming the transversality required to apply the Exchange Lemma. Hence, we conclude that, for sufficiently small $\varepsilon > 0$, the perturbed trajectory enters the sphere near $\overline{u}_0 = -1$ and exits near $\overline{u}_0 = 1$, producing a profile connecting the left and right states. Although the current case is not illustrated, it follows the construction of Section 5.1 in reverse, as shown in the case illustrated previously.

Remark 3. *Regardless of the sign of a, we have the relation $\rho = \frac{\rho_0}{\varepsilon} = \frac{\overline{\rho}_0}{\overline{\varepsilon}}$. Therefore, when the inner solution passes through the point $\overline{\rho}_0 = 1, \overline{u}_0 = 0, \overline{\varepsilon} = 0$, we observe that the variable ρ becomes unbounded due to division by $\overline{\varepsilon} = 0$. This corresponds to a singular behavior in the original physical variables, where the density becomes infinite, signaling the presence of a delta-shock and is consistent with the shadow wave approximation that predicts concentration phenomena in the singular limit $\varepsilon \to 0$.*

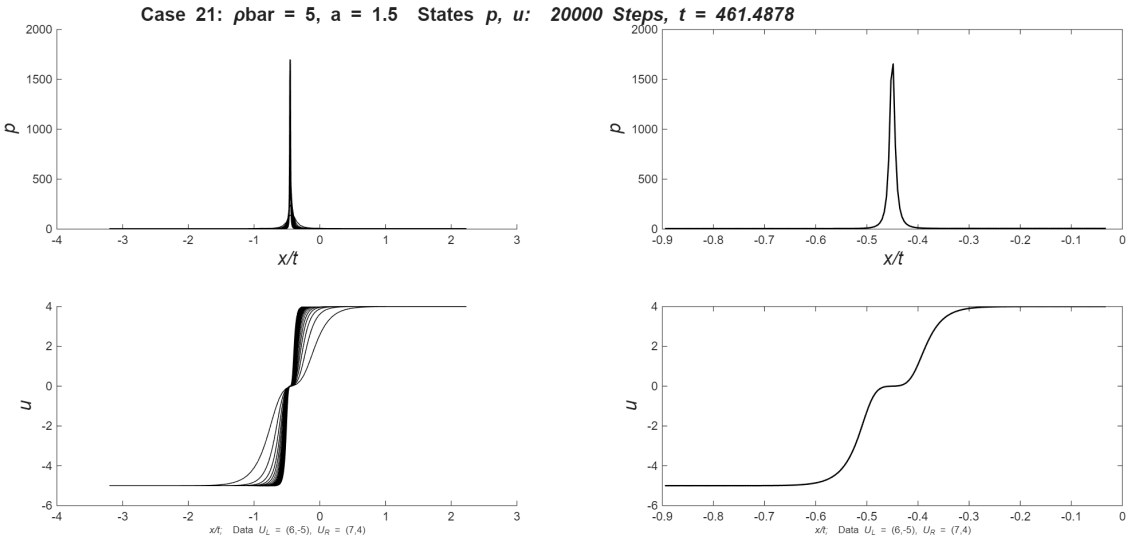

Figure 17: Right State: (6,-5). Region IV. S_δ for $a > 0$

A second delta-shock is shown numerically, in Figure 17 for Case 21. In this scenario, $\rho_L > \overline{\rho}$, $u_L < 0$, and $a = 1.5$. Similar to Case 6, the solution shows the density forming a progressively narrower, taller peak at the interface, indicating once again, convergence toward a delta-shock solution as the left state connects to the right state (albeit this time u is monotonically increasing). The shock occurs within a smaller time frame than Case 6; additionally, the magnitude of the shock is greater than twice that of Case 6 (c.f. Figure 16). However, the general structure of the shock is similar, and the explosive nature of ρ in comparison to the other solution types is apparent.

6 Conclusion

In this work, we study the Riemann problem for a Keyfitz-Kranzer-type system without source term that models transport dynamics subject to density limitations. A loss of strict hyperbolicity gives rise to non-classical wave phenomena, including transitions through degenerate states. We analyze self-similar Riemann solutions to this system, identifying both classical wave patterns, such as shocks, rarefactions, and contact discontinuities, and non-classical features, including overcompressive delta-shocks. We address the open

question of whether classical and non-classical solutions can coexist in this system for various values of the parameter $a \in \mathbb{R} \setminus \{0\}$.

We provide an affirmative answer by identifying the regions in state space where the Riemann problem is resolved non-classically (via delta-shocks).

We rigorously verify that delta-shock solutions satisfy the system in the sense of distributions using two approaches. The first involves substituting an ansatz with Dirac delta distributions into the weak formulation and testing against smooth functions. The second approach, known as the shadow wave method, constructs smooth approximations with sharply localized internal layers that converge to singular limits. Additionally, we explain the underlying singular structure using tools from geometric singular perturbation theory (GSPT), creating a framework for analyzing the formation of singular profiles in systems exhibiting degenerate or non-hyperbolic behavior. The main result of our work is the following theorem:

Theorem 1. *Let $a \in \mathbb{R} \setminus \{0\}$, and suppose that the left and right states (ρ_L, u_L) and (ρ_R, u_R) satisfy the overcompressive condition (3.19). Then, for sufficiently small $\varepsilon > 0$, the Dafermos-regularized system admits a self-similar viscous profile $(\rho_\varepsilon, u_\varepsilon)(\xi)$ that connects the left state to the right. In the limit $\varepsilon \to 0$, this profile converges to a delta-shock solution which satisfies the equations of the original hyperbolic system in the sense of distributions. More precisely, for $a < 0$, this follows directly from the verification of (3.1) and (3.2). For $a \neq 0$, the solution can be interpreted as a shadow wave in the framework of Nedeljkov.*

The complexity of the wave structure is amplified by the lack of strict hyperbolicity and the presence of degenerate characteristic speeds, as well as by the loss of genuine non-linearity and the changing convexity of the flux. Lastly, we validate our analytical findings using numerical simulations using the Local Lax–Friedrichs scheme. Future work will investigate how these Riemann solutions can serve as building blocks for general initial data in the broader Cauchy problem.

Additionally, while the LLF method produces reasonable results in areas of ample density, the dissipative nature of the scheme causes numerically ambiguous results as density approaches zero. Going forward, we hope to implement a high-order, non-dissipative numerical scheme to better analyze the behavior of solutions in the presence of vacuums. A promising option is a class of schemes called weighted essentially non-oscillatory (WENO) methods, which offer high-resolution results and can be of third-order or fifth-order accuracy, depending on the type. We are interested in exploring WENO-JS, a specific fifth-order WENO method developed by Guang-Shan Jiang and Chi-Wang Shu.

Acknowledgments. This work is supported by the National Science Foundation under Grant Number DMS-2349040 (PI: Tsikkou). Any opinions, findings, and conclusions or recommendations expressed in this material are those of the authors and do not necessarily reflect the views of the National Science Foundation.

The authors gratefully thank Marko Nedeljkov for suggesting the problem and for his insightful discussions and guidance, which were essential to the development of this work. The authors also thank Griffin Paddock, Camden Toumbleston, and Sara Wilson for sharing their earlier MATLAB code, which served as the foundation for the numerical analysis presented in this paper, and for their valuable input, which facilitated the adaptation of the implementation to the present problem.

Author Contributions. Josh Culver: Conceptualization (supporting); Data curation (supporting); Investigation (equal); Writing - original draft (lead); Writing - review & editing (equal). Aubrey Ayres: Conceptualization (supporting); Data curation (supporting); Investigation (equal); Writing - original draft (supporting); Writing - review & editing (equal). Evan Halloran: Conceptualization (supporting); Data curation (equal); Investigation (equal); Writing - original draft (supporting); Writing - review & editing (equal). Ryan Lin: Conceptualization (supporting); Data curation (equal); Investigation (equal); Writing - original draft (supporting); Writing - review & editing (equal). Emily Peng: Conceptualization (supporting); Data curation (equal); Investigation (equal); Writing - original draft (supporting); Writing - review & editing (equal). Charis Tsikkou: Conceptualization (lead); Funding acquisition (lead); Supervision (lead); Writing - original draft (supporting); Writing - review & editing (equal).

Data Availability. The data that support the findings of this study are available from the corresponding author upon reasonable request.

Conflict of Interest Statement. The authors declare that they have no conflict of interest.

References

[1] A. Aw and M. Rascle. "Resurrection of "Second Order" Models of Traffic Flow". In: *SIAM Journal on Applied Mathematics* 60.3 (2000), pp. 916–938. DOI: 10.1137/S0036139997332099. eprint: https://doi.org/10.1137/S0036139997332099. URL: https://doi.org/10.1137/S0036139997332099.

[2] F. Bouchut. "On zero pressure gas dynamics". In: *Advances in Kinetic Theory and Computing*. World Scientific, 1994, pp. 171–190.

[3] Jan Březina, Ondřej Kreml, and Václav Mácha. "Non-uniqueness of delta shocks and contact discontinuities in the multi-dimensional model of Chaplygin gas". In: *Nonlinear Differential Equations and Applications* 28.2 (Mar. 2021). Publisher Copyright: © 2021, The Author(s), under exclusive licence to Springer Nature Switzerland AG part of Springer Nature. ISSN: 1021-9722. DOI: 10.1007/s00030-021-00672-0.

[4] G.-Q. Chen and C. Klingenberg. "Hyperbolic systems of conservation laws with general flux functions having constant eigenvalues". In: *Archive for Rational Mechanics and Analysis* 135 (1996), pp. 297–354. DOI: 10.1007/BF02199833.

[5] Josh Culver, Aubrey Ayres, Evan Halloran, Ryan Lin, Emily Peng, and Charis Tsikkou. "An analysis of the Riemann problem for a 2×2 system of Keyfitz–Kranzer type balance laws with a time-dependent source term". In: *Physics of Fluids* 37.11 (Nov. 2025), p. 113340. ISSN: 1070-6631. DOI: 10.1063/5.0296696. eprint: https://pubs.aip.org/aip/pof/article-pdf/doi/10.1063/5.0296696/20816649/113340_1_5.0296696.pdf. URL: https://doi.org/10.1063/5.0296696.

[6] D. A. E. Daw and M. Nedeljkov. "Shadow waves for pressureless gas balance laws". In: *Applied Mathematics Letters* 57 (2016), pp. 54–59. ISSN: 0893-9659. DOI: https://doi.org/10.1016/j.aml.2016.01.004. URL: https://www.sciencedirect.com/science/article/pii/S0893965916300167.

[7] N. Fenichel. "Geometric singular perturbation theory for ordinary differential equations". In: *Journal of Differential Equations* 31.1 (1979), pp. 53–98. DOI: https://doi.org/10.1016/0022-0396(79)90152-9.

[8] J. Frew, N. Keyser, E. Kim, G. Paddock, C. Toumbleston, S. Wilson, and C. Tsikkou. "An analysis of a 2 × 2 Keyfitz–Kranzer type balance system with varying generalized Chaplygin gas". In: *Physics of Fluids* 36.9 (Sept. 2024), p. 096132. ISSN: 1070-6631. DOI: 10.1063/5.0231413. eprint: https://pubs.aip.org/aip/pof/article-pdf/doi/10.1063/5.0231413/20177686/096132_1_5.0231413.pdf. URL: https://doi.org/10.1063/5.0231413.

[9] T. H. Hsu. "Viscous singular shock profiles for a system of conservation laws modeling two-phase flow". In: *Journal of Differential Equations* 261.4 (2016), pp. 2300–2333. DOI: https://doi.org/10.1016/j.jde.2016.04.034.

[10] C. K. R. T. Jones. "Dynamical Systems". In: Berlin: Springer, 1995. Chap. Geomertric Singular Perturbation Theory, pp. 44–118.

[11] H. Kalisch and D. Mitrovic. "Proceedings of the Edinburgh Math Society". In: chap. Singular solutions of a fully nonlinear 2x2 system of conservation laws, pp. 711–729. DOI: https://doi.org/10.1017/S0013091512000065.

[12] B. L. Keyfitz. "Proceedings of the Fourth International Conference on Mutiphase Flow". In: 2001. Chap. Mathematical properties of non hyperbolic models for incompressible two-phase flow.

[13] B. L. Keyfitz and H. C. Kranzer. "A system of nonstrictly hyperbolic conservation laws arising in elasticity theory". In: *Archive for Rational Mechanics and Analysis* 72.3 (1980), pp. 219–241. DOI: 10.1007/BF00250863.

[14] B. L. Keyfitz, R. Sanders, and M. Sever. "Lack of hyperbolicity in the two-fluid model for two-phase incompressible flow". In: *Discrete and Continuous Dynamical Systems* 3.4 (2003), pp. 541–563. DOI: https://doi.org/10.3934/dcdsb.2003.3.541.

[15] B. L. Keyfitz, M. Sever, and F. Zhang. "Viscous singular shock structure for a nonhyperbolic two-fluid model". In: *Nonlinearity* 17.5 (2004), pp. 1731–1747. DOI: 10.1088/0951-7715/17/5/010.

[16] B. L. Keyfitz and C. Tsikkou. "Conserving the Wrong Variables in Gas Dynamics: A Riemann Solution with Singular Shocks". In: *Quarterly of Applied Mathematics* 70.3 (2012), pp. 407–436. DOI: https://doi.org/10.1090/S0033-569X-2012-01317-1.

[17] R. J. LeVeque. *Numerical methods for conservation laws*. Birkhäuser Basel, 2012, pp. 95–135. ISBN: 978-3-0348-8629-1.

[18] R. J. LeVeque, D Mihalas, E. A. Dorfi, and E. Müller. *Computational methods for astrophysical fluid flow*. Springer Berlin, Heidelberg, 1998, pp. 22–83. ISBN: 978-3-540-31632-9.

[19] H. A. Levine and B. D. Sleeman. "A system of reaction diffusion equations arising in the theory of reinforced random walks". In: *SIAM Journal of Applied Mathematics* 57.3 (1997), pp. 683–730. DOI: http://dx.doi.org/10.1137/S0036139995291106.

[20] A. Mavromoustaki and A. L. Bertozzi. "Hyperbolic systems of conservation laws in gravitydriven, particles-laden thin-film flows". In: *Journal of Engineering Mathematics* 88 (2014), pp. 29–48.

[21] M. Mazzotti. "Local equilibrium theory for the binary chromatography of species subject to a generalized Langmuir isotherm". In: *Industrial and Engineering Chemistry Research* 45.15 (2006), pp. 5332–5350. DOI: https://doi.org/10.1021/ie060297v.

[22] M. Mazzotti. "Non-classical composition fronts in nonlinear chromatography - Deltashock". In: *Indust.& Eng. Chem. Res.* 48 (2009), pp. 7733–7752.

[23] M. Mazzotti, A. Tarafder, J. Cornel, F. Gritti, and G. Guiochon. "Experimental evidence of a delta-shock in nonlinear chromatography". In: *J. Chromatography A* 1217.13 (2010), pp. 2002–2012.

[24] M. Nedeljkov. "Admissibility of a solution to generalized Chaplygin gas". In: *Theoretical and Applied Mechanics* 46.1 (2019), pp. 89–96. DOI: 10.2298/TAM190116002N.

[25] M. Nedeljkov and S. Ružičić. "On the uniqueness of solution to generalized Chaplygin gas". In: *Discrete and Continuous Dynamical Systems* 37.8 (2017), pp. 4439–4460. ISSN: 1078-0947. DOI: 10.3934/dcds.2017190.

[26] E. Yu. Panov. "On generalized entropy solutions of the Cauchy problem for a class of nonstrictly hyperbolic systems of conservation laws". In: *Sbornik Mathematics* 188.5 (1997), pp. 727–740. DOI: 10.1070/SM1997v188n05ABEH000223.

[27] D.G. Schaeffer, S. Schecter, and M. Shearer. "Nonstrictly Hyperbolic Conservation Laws with a Parabolic Line". In: *Journal of Differential Equations* 103.1 (1993), pp. 94–126. ISSN: 0022-0396. DOI: https://doi.org/10.1006/jdeq.1993.1043. URL: https://www.sciencedirect.com/science/article/pii/S0022039683710430.

[28] S. Schecter. "Existence of Dafermos profiles for singular shocks". In: *J. Differential Equations* 205.1 (2004).

[29] V. M. Shelkovich. "The Riemann problem admitting δ, δ'-shocks, and vacuum states (the vanishing viscosity approach)". In: *Journal of Differential Equations* 199.1 (2004), pp. 59–114. DOI: 10.1016/j.jde.2003.11.004.

[30] E. Tadmor. "Numerical Viscosity and the Entropy Condition for Conservative Difference Schemes". In: *Mathematics of Computation* 43.168 (1984), pp. 369–381. DOI: https://doi.org/10.2307/2008282.

[31] C. Tsikkou. "Singular shocks in a chromatography model". In: *J. Mathematical Analysis and Applications* 439.2 (2016), pp. 766–797.

[32] H. Yang and Y. Zhang. "Delta-shocks and vacuum states for the pressureless Euler equations with source terms". In: *Journal of Differential Equations* 159.2 (1999), pp. 447–484. DOI: 10.1006/jdeq.1999.3650.

[33] H. M. Zhang. "A Non-Equilibrium Traffic Model Devoid of Gas-Like Behavior". In: *Transportation Research Part B: Methodological* 36.3 (2002), pp. 275–290. DOI: 10.1016/S0191-2615(00)00048-8.

[34] Q. Zhang. "Concentration in the flux approximation limit of Riemann solutions to the extended Chaplygin gas equations with Coulomb-like friction". In: *Journal of Mathematical Physics* (2017). DOI: https://doi.org/10.1063/1.5085233.

[35] Q. Zhang. "Stability Of Riemann Solutions To Pressureless Euler Equations with Coulomb-Type Friction by Flux Approximation". In: *Electronic Journal of Differential Equations* 2019.65 (2019), pp. 1–22.